

# Design recommendations for stainless steel I-sections under concentrated transverse loading

G. B. dos Santos<sup>a,\*</sup>, L. Gardner<sup>a</sup>

<sup>a</sup> *Department of Civil and Environmental Engineering, South Kensington Campus, Imperial College London, London SW7 2AZ, UK*

## ABSTRACT

Recent investigations have highlighted the need for improved provisions for determining the resistance of stainless steel I-sections under concentrated transverse loading. Such provisions, which reflect the particular characteristics of the material, have been developed and are described herein. A review of the existing European design formulae for members under concentrated transverse loading is firstly presented. Then a series of parametric studies, based on validated finite element models are described covering I-sections with a range of web slenderness values and different stainless steel grades. On the basis of the numerical results, together with existing experimental data, revised design equations are presented and assessed through reliability analysis performed in accordance with Annex D of EN 1990. The new provisions yield enhanced ultimate load predictions and are expected to be included in the next revision of EN 1993-1-4.

**Keywords:** Concentrated transverse loading; patch loading; web crippling; Stainless steel; internal one-flange (IOF); internal two-flange (ITF); end one-flange (EOF); design standards; reliability analysis.

## Highlights (maximum 85 characters including spacing):

- Review of existing design provisions for resistance to concentrated loading
- Available test data on stainless steel I-sections under concentrated loading compiled
- Numerical parametric study performed for different stainless steel grades
- Design rules proposed for stainless steel members under concentrated loading
- Reliability analysis carried out to confirm safety of proposed design rules

## 1. INTRODUCTION

Structural steel members are often subjected to concentrated transverse loads; examples include runway beams subjected to wheel loads, columns in beam-to-column connections and bridge girders during their launching phase, as illustrated in Fig. 1(a) to Fig. 1(c). In these cases, the possibility of web bearing failure needs to be assessed. Bearing failure has been extensively studied for carbon steel I-beams [1-5] and design specifications are broadly available [6, 7]. Owing to the nonlinear stress-strain properties of stainless steel, the structural response differs from that of structural carbon steel. In strength governed scenarios, the significant strain hardening can lead to capacity benefits, while in stability governed scenarios, the early onset of nonlinearity in the stress-strain behaviour can lead to reduced capacities [8]. Previous design recommendations made by Zhao et al. [9] for the design of stainless steel hollow section members under combined axial and bending moment achieved gains of about 20% on average (greater in strength governed scenarios) over existing carbon steel design rules. Similarly to the case of members under combined loading, members under concentrated transverse loading also feature both strength and stability dominated failure modes, depending on the cross-section proportions and loading conditions; recent experimental and numerical studies on austenitic stainless steel beams [10-13] have shown that the current EN 1993-1-4 [14] design provisions are generally rather conservative. The primary aim of this paper is therefore to develop improved rules for the design of stainless steel beams under concentrated transverse loading, suitable for inclusion in the next revision of EN 1993-1-4.

In this paper, three stainless steel grades – austenitic, duplex and ferritic and three concentrated loading types are investigated herein: (i) Type (a) – internal one-flange (IOF) loading where failure occurs beneath a single concentrated load away from the beam end, (ii) Type (b) – internal two-flange (ITF) loading where failure occurs between two concentrated loads applied at opposite flanges away from the beam end and (iii) Type (c) – end-one-flange (EOF) loading where failure occurs beneath a concentrated load near the beam end, as shown in Table 1. Design provisions for each of the loading

conditions and material grades are developed, and their reliability is assessed in accordance with Annex D of EN 1990 [15].

## 2. REVIEW OF EXISTING DESIGN METHODS AND EXPERIMENTAL DATA

In this section, existing design methods for determining the resistance of hot-rolled and welded steel and stainless steel members under concentrated transverse loading are reviewed. A summary of existing experimental data on welded stainless steel sections under concentrated transverse loading is then presented.

### 2.1. ENV 1993-1-1 (1992)

The prediction of the resistance of a hot-rolled or welded steel member to concentrated transverse loading in Eurocode 3 has evolved from the ENV pre-standard [16] to the final European standard [6]. In ENV 1993-1-1 [16], the design resistance was dictated by the critical of web crippling, web crushing and web buckling. The resistance formulae for both web crushing and web crippling were devised based on a four-hinge plastic mechanism proposed by Roberts and Rockey [17, 18] whereas the web buckling resistance formula was based on idealising the web as a column. These design rules were later reformulated to align with the design approach adopted for other buckling problems in Eurocode 3 [1].

### 2.2. EN 1993-1-5 (2006)

The current European design provisions for the resistance of carbon steel members to concentrated transverse loading are set out in EN 1993-1-5. Originally proposed by Lagerqvist and Johansson [1], the design resistance to local failure under concentrated transverse loading  $F_{Rd}$  is presented as a function of the web yield strength  $f_{yw}$ , the web thickness  $t_w$ , an effective length  $L_{eff}$  and the partial safety factor  $\gamma_{M1}$ , as shown in Eq. (1):

$$F_{Rd} = \frac{f_{yw} L_{eff} t_w}{\gamma_{M1}} \quad (1)$$

The effective length  $L_{eff} = \chi_F l_y$  is given by the product of the reduction factor  $\chi_F$  and the effective loaded length, denoted  $l_y$  in general and  $l_{y,a}$ ,  $l_{y,b}$  or  $l_{y,c}$  for loading Type (a), Type (b) or Type (c)

respectively, as given by Eqs. (2)-(5), where  $s_s$  is the bearing length,  $t_f$  is the flange thickness,  $b_f$  is the flange width,  $f_{yf}$  is the flange yield strength,  $h_w$  is the web height and  $m_{2,a}$ ,  $m_{2,b}$  and  $m_{2,c}$  are the  $m_2$  factors for loading Types (a) and (b) and loading Type (c), respectively.

$$l_{y,a} = l_{y,b} = l_{y,1}, l_{y,c} = \min(l_{y,1}, l_{y,2}, l_{y,3}) \quad (2)$$

where

$$l_{y,1} = s_s + 2t_f (1 + \sqrt{m_1 + m_2}) \leq a, l_{y,2} = l_e + t_f \sqrt{\frac{m_1}{2} + \left(\frac{l_e}{t_f}\right)^2 + m_2} \text{ and } l_{y,3} = l_e + t_f \sqrt{m_1 + m_2} \quad (3)$$

in which

$$l_e = \frac{k_F E t_w^2}{2 f_{yw} h_w} \leq s_s + c \quad (4)$$

and

$$m_1 = \frac{f_{yf} b_f}{f_{yw} t_w} \text{ and } m_{2,a} = m_{2,b} = m_{2,c} = \begin{cases} 0.02 \left(\frac{h_w}{t_f}\right)^2 & \text{for } \bar{\lambda}_F > 0.5 \\ 0 & \text{for } \bar{\lambda}_F \leq 0.5 \end{cases} \quad (5)$$

The method adopted for the determination of the effective loaded length for Type (a) and Type (b) loading,  $l_{y,a}$  and  $l_{y,b}$  respectively, is based on the four-hinge plastic mechanism model proposed by Roberts and Rockey [17], whereas the effective loaded length  $l_{y,c}$  for Type (c) loading is based on different plastic mechanisms proposed by Voss [19] and modified by Lagerqvist [20].

The reduction factor  $\chi_F$ , determined from Eq. (6) is a function of the slenderness parameter  $\bar{\lambda}_F$ , which is equal to the square root of the ratio of the plastic load, given by Eq. (8), to the elastic buckling load  $F_{cr}$  of the member under concentrated force.

$$\chi_F = \frac{0.5}{\bar{\lambda}_F} \leq 1.0 \quad (6)$$

$$\bar{\lambda}_F = \sqrt{\frac{F_y}{F_{cr}}} \quad (7)$$

$$F_y = l_y t_w f_{yw} \quad (8)$$

The elastic buckling load  $F_{cr}$  is determined from Eq. (9) where  $E$  is the Young's modulus,  $k_F$  is the buckling coefficient dependent on the type of transverse loading, as given by Eq. (10),  $a$  is the distance

between web stiffeners and  $c$  is the distance between the bearing load and the member end. The definitions of the parameters  $a$  and  $c$  are also illustrated in Table 1.

$$F_{cr} = 0.9 k_F E \frac{t_w^3}{h_w} \quad (9)$$

where

$$k_F = \begin{cases} 6 + 2 \left( \frac{h_w}{a} \right)^2 & \text{for Type (a) loading} \\ 3.5 + 2 \left( \frac{h_w}{a} \right)^2 & \text{for Type (b) loading} \\ 2 + 6 \left( \frac{s_s + c}{h_w} \right) \leq 6 & \text{for Type (c) loading} \end{cases} \quad (10)$$

In the case of members subjected to concentrated transverse loading  $F$  plus bending moment  $M$  (i.e. Type (a) loading), the  $F$ - $M$  interaction is considered through Eq. (11), where  $F_{Ed}$  is the applied concentrated transverse force,  $F_{Rd}$  is the design resistance to the concentrated transverse force given by Eq. (1),  $M_{Ed}$  is the applied bending moment and  $M_{pl,Rd}$  is the plastic bending moment resistance of the cross-section, regardless of its classification (compactness). Note though that the maximum attainable bending moment resistance  $M_{Rd}$  is still limited to the plastic, elastic or effective moment capacity for Class 1-2, Class 3 and Class 4 cross-sections, respectively.

$$\frac{F_{Ed}}{F_{Rd}} + 0.8 \frac{M_{Ed}}{M_{pl,Rd}} \leq 1.4 \quad (11)$$

Recent research [2-4, 21, 22] has indicated that the design resistance model described above can be improved through adjustments to the formulae for the effective loaded length  $l_y$  and the buckling reduction factor  $\chi_F$ . The new proposals [4], which are due to be included in the next revision of EN 1993-1-5, are described in the following section.

### 2.3. RECENT DESIGN PROPOSALS FOR CARBON STEEL BY CHACÓN ET AL

Following a series of studies on the behaviour of carbon steel I-beams subjected to concentrated transverse loading [2, 3, 21, 22], two main modifications were proposed to the existing effective loaded length  $l_y$  formulae, i.e. Eqs. (2)-(5), to simplify and improve the prediction of ultimate load-carrying capacity: (i) removal of the  $m_2$  term for Type (a) and Type (b) loading cases [2, 3, 21] and (ii) removal of the yield strength ratio from the  $m_1$  term for all loading types [22], resulting in the replacement of Eq. (5) by Eq. (12).

$$m_1 = \frac{b_f}{t_w}, m_{2,a} = m_{2,b} = 0 \text{ and } m_{2,c} = \begin{cases} 0.02 \left( \frac{h_w}{t_f} \right)^2 & \text{for } \bar{\lambda}_F > 0.5 \\ 0 & \text{for } \bar{\lambda}_F \leq 0.5 \end{cases} \quad (12)$$

A new expression for the buckling reduction factor  $\chi_F$  was also proposed [4] to replace the existing plate-like resistance function of Eqs. (6)-(10) by a column-like resistance function given by Eqs. (13)-(14), with imperfection factor  $\alpha_{F0} = 0.75$  and plateau length  $\bar{\lambda}_{F0} = 0.50$ . Note that the buckling reduction factor  $\chi_F$  in Eq. (13) is to be equal to unity when  $\bar{\lambda}_F \leq \bar{\lambda}_{F0}$ .

$$\chi_F = \frac{1}{\phi_F + \sqrt{\phi_F^2 - \bar{\lambda}_F}} \text{ but } \chi_F \leq 1.0 \quad (13)$$

where

$$\phi_F = \frac{1}{2} \left[ 1 + \alpha_{F0} (\bar{\lambda}_F - \bar{\lambda}_{F0}) + \bar{\lambda}_F \right] \quad (14)$$

### 2.4. EN 1993-1-4 (2006)

For the design of stainless steel members under concentrated transverse loading, EN 1993-1-4 [14] simply refers back to the carbon steel design rules set out in EN 1993-1-5 [6]. Adoption of the carbon steel design rules, as described in Section 2.2, for the design of stainless steel members under concentrated transverse forces was originally proposed by Sélen [10] following an investigation that included nine experiments (five under Type (a) loading and four under Type (c) loading) performed

on welded I-sections made of austenitic stainless steel [11]. However, more extensive recent research [10, 12, 13] has shown a high level of conservatism in the ultimate resistance predictions of austenitic stainless steel members under all three concentrated loading types.

## 2.5. REVIEW OF EXISTING EXPERIMENTAL DATA

A total of 43 experiments on austenitic stainless steel I-section beams under three types of concentrated loading – Type (a), Type (b) and Type (c) loading have been reported in previous studies [10-13]; of these, 21 were performed under Type (a) loading, 8 under Type (b) loading and 14 under Type (c) loading. A summary of the key geometric and material properties, as well as the ultimate capacities from the tests, is shown in Table 2, where  $h$  is the overall height of the cross-section,  $L$  is the beam span,  $a$  is the clear distance between web stiffeners,  $b$  is the free distance between the loading plate and the bearing plate in the Type (c) loading configuration,  $h_w/t_w$  is the ratio between the web height (where  $h_w = h - 2t_f$ ) and the web thickness  $t_w$  and  $F_{u,test}$  is the ultimate test load at the load application point for Type (a) and Type (b) loading or at the bearing support for Type (c) loading. All tests were performed on welded austenitic stainless steel sections with web slenderness values ( $h_w/t_w$ ) ranging from 18 to 107 for Type (a) loading, 14 to 19 for Type (b) loading and 12 to 77 for Type (c) loading, as shown in Table 2. A numerical modelling program was therefore carried out to expand the structural performance database for austenitic stainless steel I-sections with a broader range of slenderness ratios [12, 13]. Further numerical results are generated in the present paper for the duplex and ferritic grades.

## 3. NUMERICAL MODELLING

A numerical modelling programme was carried out to examine the behaviour of stainless steel I-section members of different slenderness ratios under Type (a) loading, Type (b) loading and Type (c) loading (see Table 1). The nonlinear finite element software ABAQUS [23] was adopted to carry out the numerical analyses. A comprehensive description of the finite element models and their validation against experimental results were presented by the authors in previous publications [12, 13]; hence, only a summary of key features of the modelling are presented in this section. While austenitic stainless steel I-sections under concentrated loading have been examined experimentally and numerically in

previous research, equivalent studies have yet to be performed on the duplex and ferritic stainless steel grades. This is addressed in the numerical study presented in this section.

### **3.1. MODELLING ASSUMPTIONS AND VALIDATION**

The four-noded doubly curved shell element with reduced integration and finite membrane strain, referred to as S4R in the Abaqus element library [23], was adopted to simulate the studied stainless steel I-beams, end plates and web stiffeners, whereas the eight-noded linear solid element with reduced integration, referred to as C3D8R in the Abaqus element library [23], was used to model the bearing plates. An element size equal to half of the cross-sectional web thickness was adopted for the I-section members, end plates and web stiffeners, following a preliminary mesh sensitivity study. A typical FE model is shown in Fig. 2. For the validation of the numerical models, the existing tests on austenitic stainless steel members summarised in Section 2.5 were utilised, where the measured material stress-strain properties [24] (converted into true stress-strains as explained in Section 3.2) were adopted. The material modelling approach adopted in the parametric studies on duplex and ferritic stainless steel sections is described in Section 3.2.

The boundary conditions of the developed FE models were defined to reflect the test setups and previous numerical validation studies described by dos Santos et al [12] and dos Santos and Gardner [13], as shown in Table 4. The bearing and loading plates were simulated as rigid blocks. For the Type (a) loading model, the vertical (U2) and out-of-plane (U1) displacements, as well as the rotations about the vertical (UR2) and longitudinal (UR3) axes at the bottom of each end plate were restrained, as shown in Table 4. For the Type (b) loading model, the out-of-plane displacement (U1) was restrained at four end plate nodes, as also shown in Table 4. Both the Type (a) and Type (b) loading models had their longitudinal displacement (U3) restrained at the mid-length of the top flange to provide symmetry in the boundary conditions, similar to the tests [12, 13]. For the Type (c) loading model, the bearing plate (at the right-hand support) was restrained in the transverse (U1) and vertical (U2) directions, and rotations about the vertical (UR2) and longitudinal (UR3) axes were also prevented. The loading plate (at the top flange) had its transverse (U1) and longitudinal (U3) displacements, and its rotations about

the vertical (UR2) and longitudinal (UR3) axes, restrained, as shown in Table 4. The longitudinal displacement was initially restrained ( $U3 = 0$ ) at the left-hand support, but the restraint was removed ( $U3$  free) once contact between the loading plate and the top flange of the I-beam, as well as between the bearing plate and the bottom flange of the I-beam, had been established.

The contact interaction between the bearing plate and loading plates (master surfaces) and the I-section flanges (slave surfaces) was simulated using a finite sliding procedure [23]. A friction coefficient of 0.4 was used for the tangential contact properties while a “hard” contact relationship was adopted for the normal contact properties, assuming that the contact pressure-overclosure relationship is dictated by the stiffness of each of the parts in contact with each other [23].

The accuracy of finite element models in predicting the ultimate load-carrying capacity of members under concentrated transverse forces was previously assessed [12, 13] by comparing numerical results with those obtained by tests. In these studies, it was found that welded stainless steel I-sections under concentrated transverse loading have very low sensitivity to residual stresses [12, 13], which can hence be omitted from numerical models, and that an imperfection pattern corresponding to the first elastic buckling mode shape obtained from a linear eigenvalue analysis with an imperfection amplitude  $\omega$  of 1/500 of the web thickness provided an accurate representation of test behaviour. A similar approach was therefore adopted herein. Geometrically and materially non-linear analyses with imperfections (GMNIA) were then carried out using the general static solver [23] with displacement control. A detailed description of the validation of the finite element models of austenitic stainless steel I-sections subjected to Type (a) and Type (b) loading was presented by dos Santos *et al.* [12], while for Type (c) loading was examined by dos Santos and Gardner [13]. A summary of the validation results for all three loading cases is shown in Table 5. The test results used for the FE model validation are also used in Section 4 for the assessment of design provisions.

### 3.2. PARAMETRIC STUDIES

For the austenitic stainless steel members, results from previously conducted parametric studies [12, 13] were used for all three investigated loading types. For the duplex and ferritic stainless steel members, the stress-strain behaviour was represented by the two-stage Ramberg-Osgood (R-O) material model [25], as given by Eqs. (15) and (16), where  $\varepsilon$  and  $f$  are the engineering strain and stress respectively,  $E$  is the Young's modulus,  $E_{0.2}$  is the tangent modulus at the 0.2% proof stress,  $f_y$  is the 0.2% proof stress,  $\varepsilon_{t,0.2}$  is the total strain at the 0.2% proof stress,  $\varepsilon_u$  is the strain at the ultimate tensile stress and  $n$  and  $m$  are strain hardening coefficients. The standardised values for the key parameters of the material stress-strain curves recommended in [26] were adopted for the duplex and ferritic grades, a summary of which is given in Table 3.

$$\varepsilon = \frac{f}{E} + 0.002 \left( \frac{f}{f_y} \right)^n \quad \text{for } f \leq f_y \quad (15)$$

$$\varepsilon = \frac{f - f_y}{E_{0.2}} + \left( \varepsilon_u - \varepsilon_{t,0.2} - \frac{f_u - f_y}{E_{0.2}} \right) \left( \frac{f - f_y}{f_u - f_y} \right)^m \quad \text{for } f \leq f_y \quad (16)$$

The engineering material stress-strain curves, obtained either from coupon tests or the Ramberg-Osgood model, were converted into true stress and log plastic strain according to Eqs. (17) and (18), where  $\sigma_{\text{true}}$  is the true stress,  $\varepsilon_{\text{ln}}^{\text{pl}}$  is the true plastic strain, and  $\sigma_{\text{nom}}$  and  $\varepsilon_{\text{nom}}$  are the engineering stress and engineering strain respectively. The adopted engineering stress-strain curves and the corresponding true stress-strain curves for the modelled austenitic, duplex and ferritic stainless steels are shown in Fig. 3.

$$\sigma_{\text{true}} = \sigma_{\text{nom}} (1 + \varepsilon_{\text{nom}}) \quad (17)$$

$$\varepsilon_{\text{ln}}^{\text{pl}} = \ln(1 + \varepsilon_{\text{nom}}) - \frac{\sigma_{\text{true}}}{E} \quad (18)$$

All modelled cross-sections had a web height  $h_w$  of 410 mm or 250 mm, flange width  $b_f$  of 150 mm, flange thickness  $t_f$  of 20 mm and bearing length  $s_s$  of 20 mm or 35 mm. For Type (a) loading, the member length ( $L$ ) was also varied from 600 mm to 2100 mm to consider the effects of combined concentrated transverse force and bending moment. For Type (b) loading, the distance between web

stiffeners  $a$  were kept constant at 600 mm and for Type (c) loading, the distance between the web stiffener and the bearing plate  $b$  was kept constant at 615 mm. For all loading and material types, the web thickness was varied to cover slenderness values  $\bar{\lambda}_F$  from 0.30 to 3.00.

#### 4. ASSESSMENT OF EXISTING DESIGN METHODS AND NEW DESIGN PROPOSAL

In this section the available test and numerical data are used to evaluate the accuracy of the design provisions in EN 1993-1-4 [14], the design procedure proposed by Chacón *et al.* [4] and a new design proposal for stainless steel members under concentrated transverse loading. The accuracy of the design predictions is evaluated by comparing the numerical or test failure load ( $F_u$ ) with the ultimate load predicted by the design procedure ( $F_{Rd,pred}$ ) for austenitic, duplex and ferritic stainless steel members under three types of concentrated loading – Type (a), (b) and (c) loading. Four Type (c) tests and one Type (a) test, indicated by an  $\times$  in Table 2, were not considered in the evaluation due to their critical design check relating to bending plus shear failure rather than failure under concentrated loading. Similarly, two Type (a) tests, identified with an  $*$  in Table 2, were not considered due to their critical design check relating to shear failure. An additional criterion for excluding test or numerical data from the performance evaluation of the studied design formulae was when, for members subjected to Type (a) loading, the effective loaded length  $l_y$  exceeded the distance between the web stiffeners (i.e. distance  $a$  in Table 1) though such cases did not arise in the geometries considered in this investigation. This additional criterion is based on the findings presented in [27, 28], where a change in failure mode was observed in cases of  $a/h$  values less than about 1.0. The lowest  $a/h$  ratios arising in the specimens examined in the present study was 1.29.

To account for the combined bending moment and concentrated loading that arises under Type (a) loading, the design interaction curve given by Eq. (11) was used, where the test or numerical failure load  $F_u$  corresponds to the distance on the F-M interaction diagram from the origin to the test or numerical data point whereas the predicted design load  $F_{u,pred}$  corresponds to the distance on the interaction diagram from the origin to the intersection with the design curve, assuming proportional

loading, as shown in Fig. 4. Note that all partial safety factors were set equal to unity for comparison purposes.

#### 4.1. EN 1993-1-4 [14]

The existing test results summarised in Section 2.5, together with the parametric numerical data generated herein and in [12, 13], were used to evaluate the current design provisions of EN 1993-1-4 [14] for stainless steel members under concentrated transverse loading. The full set of data is shown in Fig. 5 in terms of the ultimate capacity  $F_u$  normalized by the EN 1993-1-4 predicted resistance  $F_{u,EC3}$ , grouped by stainless steel type in Fig. 5(a) and grouped by loading type in Fig. 5(b). A quantitative evaluation of the mean  $F_u/F_{u,EC3}$  value and the COV of all data points is presented in Table 6 by loading type and slenderness. All data points are located above the unity line in Fig. 5, showing that conservative results were obtained throughout the entire slenderness range for all three loading types. Average underpredictions of capacity of approximately 50% for Types (a) and (c) loading and 75% for Type (b) loading were obtained. Similar results were obtained by S elen [10] - i.e. an average of 34% underprediction of capacity for Type (a) loading and 46% for Type (c) loading. The underpredictions of capacity are observed throughout the slenderness range and are associated with the inherent difference in stress-strain curve behaviour of stainless steel and carbon steel. The underpredictions of capacity are particularly evident in the stocky slenderness range ( $\bar{\lambda}_F \leq \bar{\lambda}_{F0}$ ). The test and numerical data on stainless steel members under concentrated loading are also plotted in terms of the buckling reduction factor  $\chi_F$  versus slenderness  $\bar{\lambda}_F$  in Fig. 6. Note that data for members subjected to Type (a) loading with  $M_u \geq 0.5M_{pl,Rd}$  are not included in Fig. 6. The latter figure shows significant conservatism throughout the entire slenderness range, with clear scope for improvement.

#### 4.2. CHAC ON ET AL. [4]

The design approach developed by Chac on et al [4] for carbon steel members subjected to concentrated loading, including a new definition for the effective loaded length  $l_y$  for Type (a) and Type (b) loading and new buckling curves, as described in Section 2.3, is assessed herein. The ratio between the test or

numerical resistances  $F_u$  and the resistance predicted using the approach of Chacón et al,  $F_{u,Chacón}$  as given by Eqs. (12)-(14), is plotted against slenderness  $\bar{\lambda}_F$  in Fig. 7, where the data are grouped by stainless steel type in Fig. 7(a) and by loading type in Fig. 7(b). A value greater than unity indicates a safe-sided prediction. A quantitative evaluation of the mean and COV values for the  $F_u/F_{u,Chacón}$  ratio is presented in Table 7. The former shows a slight improvement, particularly for higher values of slenderness  $\bar{\lambda}_F$ , over EN 1993-1-4, with  $F_u/F_{u,Chacón}$  mean values of 1.45, 1.74 and 1.40 for Types (a), (b) and (c) loading, respectively – see Table 6. However, there still remains considerable scope for improvements in the ultimate capacity predictions of stainless steel members subjected to concentrated loading, as presented in Section 4.3.

### 4.3. NEW DESIGN RULES FOR STAINLESS STEEL

The improved design rules proposed in this section for stainless steel are based on Chacon et al's [4] resistance function, which ensures compatibility of design approach between stainless steel and carbon steel members in the next revision of Eurocode 3, but with the  $\alpha_{F0}$  and  $\bar{\lambda}_{F0}$  parameters calibrated for stainless steel. The calibration is carried out based on data from the 39 test results and 369 numerical results reported in Sections 2.5 and 3, respectively. In the new design proposal, the buckling reduction factor  $\chi_F$  is given by Eq. (13), with the parameter  $\phi_F$  defined by Eq. (14) and slenderness  $\bar{\lambda}_F$  given by Eq. (7). The critical buckling load  $F_{cr}$  and the buckling coefficient  $k_F$  for each loading type are given by Eq. (9) whereas the plastic collapse load  $F_y$  is given by Eq. (8). The effective loaded length  $l_y$  is given by Eqs. (2)-(4), with values of  $m_1$  and  $m_2$  given by Eq. (12). Following analysis of the test and numerical data, new imperfection factor  $\alpha_{F0}$  and plateau length  $\bar{\lambda}_{F0}$  values are proposed in Table 8 according to the loading type and stainless steel grade. The ratios between the test and numerical ultimate loads  $F_u$  and the proposed ultimate resistances  $F_{u,prop}$  are plotted in Fig. 9 as a function of slenderness, with data grouped by stainless steel type in Fig. 9(a) and by loading type in Fig. 9(b). The mean and COV values of the  $F_u/F_{u,prop}$  ratios for the different loading types and material grades

are shown Table 9. The new design proposals bring consistent improvements for Type (a) and Type (b) loading, and the same result for Type (c) loading. A comparison of the EN 1993-1-4, Chacón *et al.* [4] and new proposed strength curves are presented in Fig. 10 to Fig. 12, where the data are presented in groups of the same proposed  $\alpha_{F0}$  and  $\bar{\lambda}_{F0}$  values: austenitic and duplex stainless steel members under Type (a) and Type (b) loading are shown in Fig. 10; ferritic stainless steel members under Type (a) and Type (b) loading are shown in Fig. 11 and all stainless steel members under Type (c) loading are shown in Fig. 12.

The members subjected to Type (a) loading with  $M_u \geq 0.5M_{pl,Rd}$  have not been included in the comparisons presented thus far to allow the effect of concentrated transverse loading to be assessed in isolation. These data points are now assessed using the interaction curve given by Eq. (11), as presented in Fig. 13, where  $F_u$  and  $M_u$  are the ultimate load and moment respectively from the Type (a) loading tests and numerical models,  $F_{u,prop}$  is the ultimate load predicted using the proposals made in this section and  $M_{pl,Rd}$  is the plastic bending resistance of the cross-section, regardless of its classification. The design interaction curve may be seen to provide consistently safe-sided predictions with the proposed end-point for resistance to concentrated transverse loading  $F_{u,prop}$ . The high scatter observed in Fig. 13 is related primarily to stainless steel members with stocky cross-sections ( $\bar{\lambda}_F < 0.6$ ) due to the difference in shape between the resistance function and the actual behaviour of the specimen under concentrated loading, as also observed in Fig. 9.

Overall, the proposed design rules are consistent with the new provisions for carbon steel sections subjected to concentrated transverse loading due to be incorporated into the next revision of EN 1993-1-5, feature new imperfection factors and plateau length values that reflect the particular characteristics of stainless steel and result in average enhancements in efficiency of about 20% for Type (a) loading and 10% for Type (c) loading.

#### 4.4. RELIABILITY ANALYSIS

An assessment of the reliability of the proposed design equations for predicting the ultimate capacity of stainless steel members under concentrated transverse forces, as set out in Section 4.3, was performed according to Annex D of EN 1990 [15]. Reliability analyses were carried out on the following 12 groups of data: one for each material grade, i.e. austenitic, duplex and ferritic, and for each loading type – i.e. Type (a) loading with  $M_u \geq 0.5M_{Rd}$  (accounting for interaction between bending and concentrated loading), Type (a) loading with  $M_u < 0.5 M_{Rd}$  (no interaction between bending and concentrated loading), Type (b) loading and Type (c) loading. Furthermore, each data group was divided into two sub-sets based on slenderness  $\bar{\lambda}_F$  – the first sub-set covered the stocky range (i.e.  $\bar{\lambda}_F \leq \bar{\lambda}_{F0}$ ), while the second sub-set focussed on the proposed resistance functions for  $\bar{\lambda}_F > \bar{\lambda}_{F0}$ . A key reason for considering the data in sub-sets is to reflect the different structural behaviour found in different slendernesses ranges. This has been observed elsewhere [27, 28] and, in this context of the present paper, is manifested by high ratios of  $F_u/F_{u,prop}$  accompanied by high scatter in the stocky range ( $\bar{\lambda}_F \leq \bar{\lambda}_{F0}$ ) and lower  $F_u/F_{u,prop}$  values accompanied by lower scatter in the slender range ( $\bar{\lambda}_F > \bar{\lambda}_{F0}$ ). Considering the two sub-sets in isolation, as permitted in Annex D of EN 1990 [15], enables favourable  $\gamma_M$  values to be obtained, while considering the two sub-sets together as a single dataset can yield excessively conservative results.

The procedure described in Annex D of EN 1990 requires that the assessed resistance function  $F_{Rd}$  contains only independent variables. Eq. (1) is therefore rewritten in the form presented in Eq. (19) where  $t_w$  and  $f_{yw}$  are the independent (or basic) variables,  $k$  is a constant which does not depend  $t_w$  or  $f_{yw}$  and the powers  $d$  and  $e$  are model parameters which should be determined for each specimen according to the approach described below.

$$F_{Rd} = k t_w^d f_{yw}^e \quad (19)$$

Considering two beams with the same web thickness  $t_w$  but different web yield strengths  $f_{yw,1}$  and  $f_{yw,2}$ , the ratio of their resistances to concentrated transverse loading is given by Eq. (20).

$$\frac{F_{Rd,2}}{F_{Rd,1}} = \frac{k t_w^d f_{yw,2}^e}{k t_w^d f_{yw,1}^e} = \left( \frac{f_{yw,2}}{f_{yw,1}} \right)^e \quad (20)$$

Hence, the power  $e$  may be calculated as follows:

$$e = \frac{\ln\left(\frac{F_{Rd,2}}{F_{Rd,1}}\right)}{\ln\left(\frac{f_{yw,2}}{f_{yw,1}}\right)} \quad (21)$$

The power  $d$  is subsequently determined from Eq. (22) by considering two beams with different web thicknesses  $t_{w,1}$  and  $t_{w,2}$ .

$$d = \frac{\ln\left(\frac{F_{Rd,2}}{F_{Rd,1}}\right) - e \ln\left(\frac{f_{yw,2}}{f_{yw,1}}\right)}{\ln\left(\frac{t_{w,2}}{t_{w,1}}\right)} \quad (22)$$

Owing to the complex form of the resistance function for members under concentrated transverse forces  $F_{Rd}$ , the variability of the basic variables  $t_w$  and  $f_{yw}$  for different slenderness values is given by Eq. (23), where  $g_{rt}^2(\underline{X}_m)$  and  $\text{VAR}[g_{rt}(\underline{X})]$  are the mean and variance of the resistance function  $g_{rt}(\underline{X})$  given in Eq. (19),  $\sigma_{t_w}$  and  $\sigma_{f_{yw}}$  are the standard deviations of the web thickness and the web yield strength respectively,  $t_{w,m}$  and  $f_{yw,m}$  are the mean values of the web thickness and the web yield strength respectively and  $V_{t_w}$  and  $V_{f_{yw}}$  are the coefficients of variation of the web thickness and the web yield strength, respectively.

$$\begin{aligned}
V_{rt}^2 &= \frac{\text{VAR}[g_{rt}(\underline{X})]}{g_{rt}^2(\underline{X}_m)} \cong \frac{1}{g_{rt}^2(\underline{X}_m)} \times \sum_{i=1}^j \left( \frac{\partial g_{rt}}{\partial X_i} \sigma_i \right)^2 \\
&= \frac{1}{g_{rt}^2(\underline{X}_m)} \left[ \left( \frac{\partial g_{rt}}{\partial t_w} \sigma_{t_w} \right)^2 + \left( \frac{\partial g_{rt}}{\partial f_{yw}} \sigma_{f_{yw}} \right)^2 \right] \\
&= \frac{1}{g_{rt}^2(\underline{X}_m)} \left[ \left( d t_w^{d-1} f_{yw}^e \sigma_{t_w} \right)^2 + \left( e f_{yw}^{e-1} t_w^d \sigma_{f_{yw}} \right)^2 \right] \\
&= \frac{1}{g_{rt}^2(\underline{X}_m)} \left[ \left( d \frac{g_{rt}}{t_w} \sigma_{t_w} \right)^2 + \left( e \frac{g_{rt}}{f_{yw}} \sigma_{f_{yw}} \right)^2 \right] \\
&= \frac{g_{rt}^2(\underline{X}_m)}{g_{rt}^2(\underline{X}_m)} \left[ \left( d \frac{\sigma_{t_w}}{t_{w,m}} \right)^2 + \left( e \frac{\sigma_{f_{yw}}}{f_{yw,m}} \right)^2 \right] \\
&= \left( d V_{t_w} \right)^2 + \left( e V_{f_{yw}} \right)^2
\end{aligned} \tag{23}$$

Based on previous research into the mechanical and geometrical properties of stainless steel structural sections [29], the variability of the web yield strength  $V_{f_{yw}}$  was taken as 0.060, 0.030 and 0.045 for austenitic, duplex and ferritic stainless steel respectively, and the variability of the web thickness  $V_{t_w}$  was taken equal to 0.05. Over-strength factors for the material yield strength  $f_{y,mean}/f_{y,min}$ , where  $f_{y,mean}$  is the mean yield strength and  $f_{y,min}$  is the minimum specified yield strength, of 1.30, 1.10 and 1.20 for austenitic, duplex and ferritic stainless steel respectively, were also adopted based on the recommendations of Afshan *et al.* [29].

A summary of the key statistical parameters and the results of the reliability analyses are presented in Table 10 for each combination of material grade and loading type, where  $n$  is the number of test and FE results under consideration,  $b$  is the average ratio of test or FE ultimate capacity  $F_u$  to proposed ultimate design resistance  $F_{u,prop}$ ,  $V_\delta$  is the variation of the error in the prediction of ultimate load,  $V_{FEM}$  is an artificial coefficient of variation relating to the use of numerical results and determined by considering the variation between the experimental and numerical results presented by dos Santos *et al.* [12] and dos Santos and Gardner [13],  $V_r$  is the coefficient variation of the resistance function given by Eq. (24) and  $k_{d,n}$  is the design fractile factor given in EN 1990 [15]. Note that  $n$  corresponds to the number of cases where  $\bar{\lambda}_F > \bar{\lambda}_{F0}$ , except for Type (a) loading cases with  $M_u \geq 0.5M_{pl}$  where  $n$

corresponds to the total number of cases. Also note that  $k_{d,n}$  was obtained based on the total number of tests and FE models in each of the twelve sub-sets analysed, in accordance with EN 1990 [15].

$$V_r = \sqrt{V_\delta^2 + V_{rt}^2 + V_{FEM}^2} \quad (24)$$

The required values for the partial safety factor  $\gamma_{M1}$  are lower than 1.10, which is the partial safety factor adopted in EN 1993-1-4 for the design of stainless steel members under concentrated loading. Therefore the proposed design equations presented in Section 4.3 with partial safety factor  $\gamma_{M1} = 1.10$  can be safely applied to the design of stainless steel members under concentrated transverse loading.

## 5. CONCLUSIONS

The design of stainless steel members subjected to concentrated transverse loading has been investigated in this study. Firstly a review of existing design methods was presented and relevant experimental data from the literature were summarised. Additional data covering the three main families of stainless steel and three concentrated loading conditions were then generated by means of numerical parametric studies. In total, 39 test results and 366 numerical results were then used to assess the current design provisions in EN 1993-1-4 [14], the design method of Chacón et al [4] for carbon steel members and a proposed new design approach. The new design proposals are in line with the method of Chacón et al, enabling consistency between the treatment of carbon steel and stainless steel in the next revision of Eurocode 3, reflect the particular characteristics of stainless steel and offer 10-20% improvements in capacity predictions over existing methods. The reliability of the proposed design expressions was demonstrated in accordance with EN 1990 [15].

## 6. ACKNOWLEDGMENT

The financial support of the Brazilian National Council for Scientific and Technological Development (CNPq, Brazil) is gratefully acknowledged.

## REFERENCES

- [1] Lagerqvist, O. and Johansson, B. "Resistance of I-girders to concentrated loads". *Journal of Constructional Steel Research*, 39 (2): p. 87-119, 1996.
- [2] Gozzi, J. "Patch loading resistance of plated girders - Ultimate and serviceability limit state". *Department of Civil, Mining and Environmental Engineering*, Luleå University of Technology, PhD thesis, 2007.
- [3] Davaine, L. "Formulation de la résistance au lancement d'une âme métallique de pont raidie longitudinalement". Institut National des Sciences Appliquées, PhD thesis (D05-05): p. 270, 2005.
- [4] Chacón, R., Braun, B., Kuhlmann, U., and Mirambell, E. "Statistical evaluation of the new resistance model for steel plate girders subjected to patch loading". *Steel Construction*, 5 (1), 2012.
- [5] Graciano, C. "Patch loading resistance of longitudinally stiffened girders - A systematic review". *Thin-Walled Structures*, 95: p. 1-6, 2015.
- [6] EN 1993-1-5:2006. *Eurocode 3: Design of steel structures - Part 1-5: Plated structural elements*, European Committee for Standardization (CEN), Brussels, 2006.
- [7] EN 1993-6:2007. *Eurocode 3 - Design of steel structures - Part 6: Crane supporting structures*, BSI, Brussels, 2007.
- [8] Gardner, L. "Stability and design of stainless steel structures - Review and outlook". *Thin-Walled Structures*, 141: p. 208-216, 2019.
- [9] Zhao, O., Gardner, L., and Young, B. "Structural performance of stainless steel circular hollow sections under combined axial load and bending - Part 2: Parametric studies and design". *Thin-Walled Structures*, 101: p. 240-248, 2016.
- [10] Sélen, E. "Work package 3.5 - Final Report - Web crippling". Report to the ECSC Project - Development of the use of stainless steel in construction. Contract no. 7210-SA/903, Lulea University of Technology, 2000.
- [11] Unosson, E. "Patch loading of stainless steel girders". *Department of Civil and Mining Engineering*, Lulea University of Technology, Bachelor, 2003.
- [12] dos Santos, G.B., Gardner, L., and Kucukler, M. "Experimental and numerical study of stainless steel I-sections under concentrated internal one-flange and internal two-flange loading". *Engineering Structures*, 175: p. 355-370, 2018.
- [13] dos Santos, G.B. and Gardner, L. "Testing and numerical analysis of stainless steel I-sections under concentrated end-one-flange loading". *Journal of Constructional Steel Research*, 157: p. 271-281, 2019.

- [14] EN 1993-1-4:2006+A1:2015. *Eurocode 3: Design of steel structures - Part 1.4: General rules - Supplementary rules for stainless steels*, European Committee for Standardization (CEN), Brussels, 2006.
- [15] EN 1990:2002+A1. *Eurocode - Basis of structural design*, 2005.
- [16] ENV 1993-1-1:1992. *Eurocode 3: Design of steel structures - Part 1.1: General rules and rules for buildings*, European Committee for Standardization (CEN), Brussels, 1992.
- [17] Roberts, T.M. and Rockey, K.C. "A mechanism solution for predicting the collapse loads of slender plate girders when subjected to in-plane patch loading". *Proceedings of the Institution of Civil Engineers, Part 2*, 67: p. 155-175, 1979.
- [18] Roberts, T.M. and Rockey, K.C. "A mechanism solution for predicting the collapse loads of slender plate girders when subjected to in-plane patch loading (Discussion)". *Proceedings of the Institution of Civil Engineers, Part 2*, 69: p. 577-579, 1980.
- [19] Voss, R.-P. "Bemessung von Lasteinleitungssteifen in geschweißten Vollwandträgern (Dimensioning of load-introduction-stiffeners in welded plate girders, in German)". *Stahlbau*, 56 (4): p. 97-106, 1987.
- [20] Lagerqvist, O. "Patch loading - Resistance of steel girders to concentrated forces". *Division of Steel Structures*, Lulea University of Technology, PhD thesis (1994:159D), 1995.
- [21] Clarin, M. "Plate Buckling Resistance - Patch Loading of Longitudinally Stiffened Webs and Local Buckling". Lulea University of Technology, Doctoral degree (2007:31), 2007.
- [22] Chacón, R., Mirambell, E., and Real, E. "Hybrid steel plate girders subjected to patch loading, Part 2: Design proposal". *Journal of Constructional Steel Research*, 66: p. 709-715, 2010.
- [23] ABAQUS. "Abaqus version 6.14". SIMULIA - Dassault Systèmes [Software] 2014.
- [24] Gardner, L., Bu, Y., and Theofanous, M. "Laser-welded stainless steel I-sections: Residual stress measurements and columns buckling tests". *Engineering Structures*, 127: p. 536-548, 2016.
- [25] Arrayago, I., Real, E., and Gardner, L. "Description of stress-strain curves for stainless steel alloys". *Materials and Design*, 87: p. 540-552, 2015.
- [26] Afshan, S., Zhao, O., and Gardner, L. "Standardised material properties for numerical parametric studies of stainless steel structures and buckling curves for tubular columns". *Journal of Constructional Steel Research*, 152: p. 2-11, 2019.
- [27] Chacón, R., Mirambell, E., and Real, E. "Transversally stiffened plate girders subjected to patch loading. Part 1. Preliminary study". *Journal of Constructional Steel Research*, 80: p. 483-491, 2013.

- [28] Chacón, R., Mirambell, E., and Real, E. "Transversally stiffened plate girders subjected to patch loading: Part 2. Additional numerical study and design proposal". *Journal of Constructional Steel Research*, 80: p. 492-504, 2013.
- [29] Afshan, S., Francis, P., Baddoo, N.R., and Gardner, L. "Reliability analysis of structural stainless steel design provisions". *Journal of Constructional Steel Research*, 114: p. 293-304, 2015.

# FIGURES

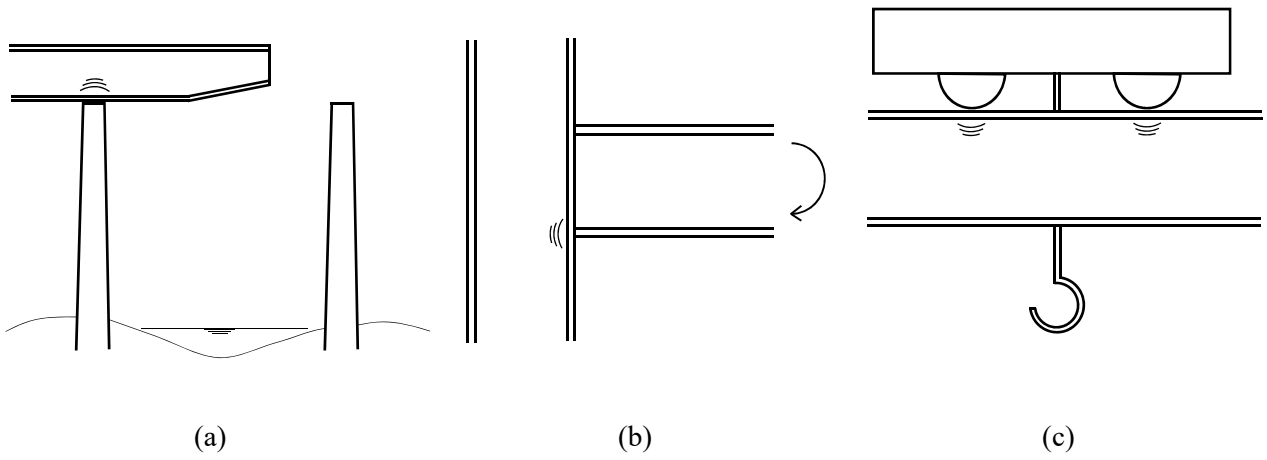


Fig. 1. Practical cases susceptible to web bearing failure.

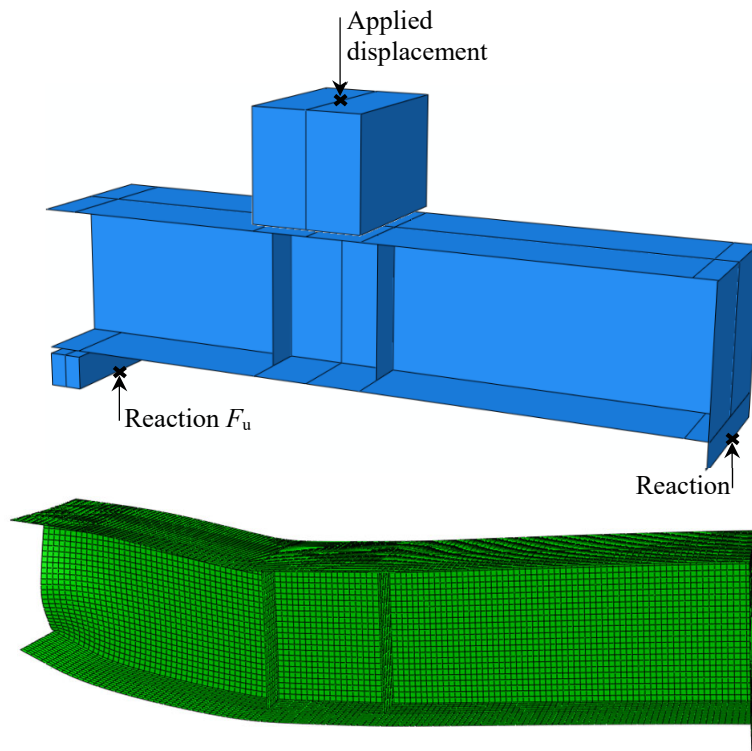


Fig. 2. Finite element model and typical deformed shape under Type (c) loading for EOF-h140-b180-ss30-c0 specimen [13].

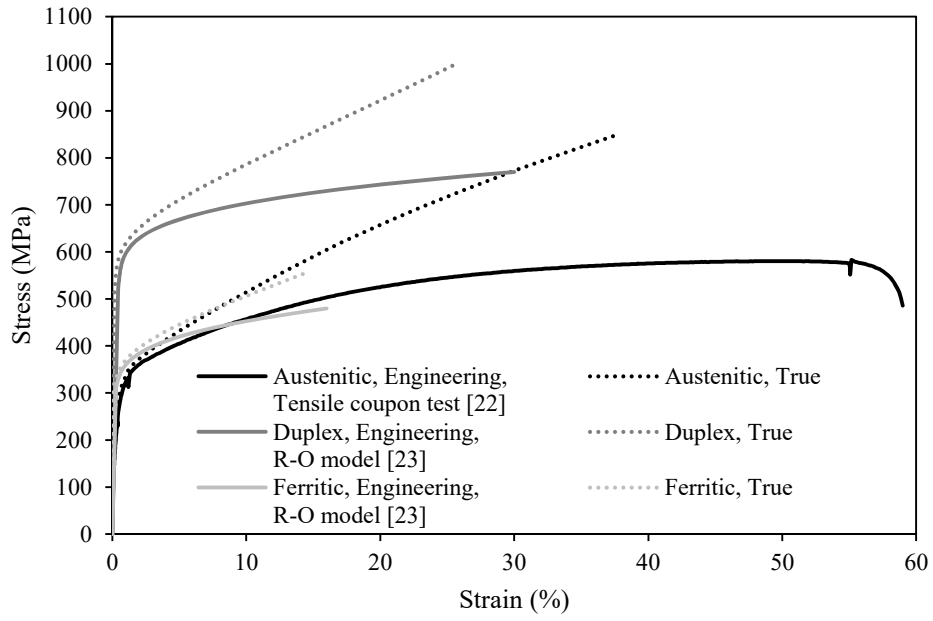


Fig. 3. Engineering and true stress-strain curves for austenitic, duplex and ferritic stainless steel.

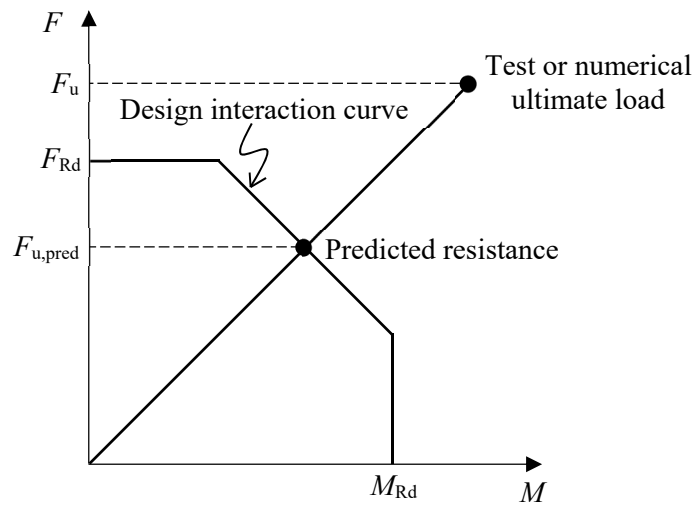


Fig. 4. Definition of  $F_u$  and  $F_{u,pred}$  for Type (a) loading.

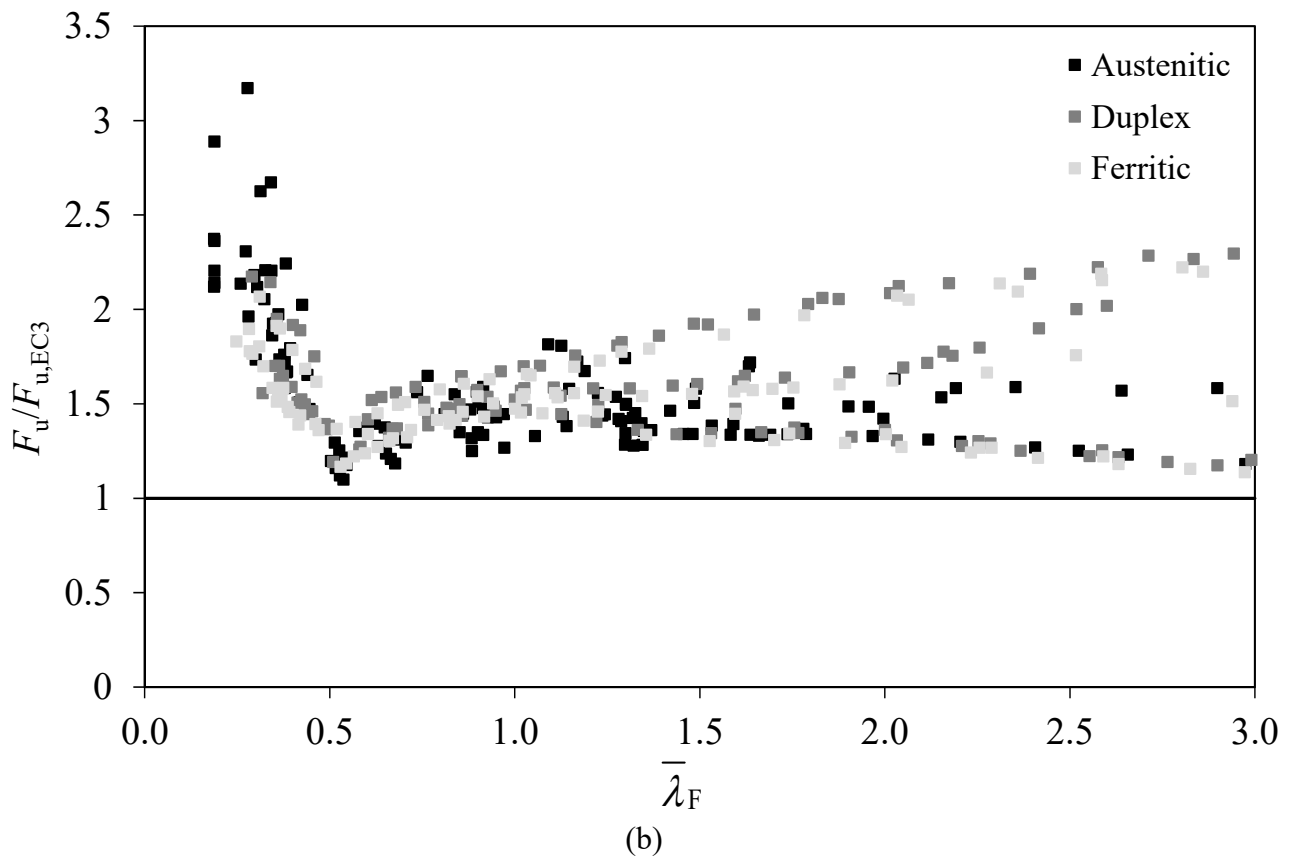
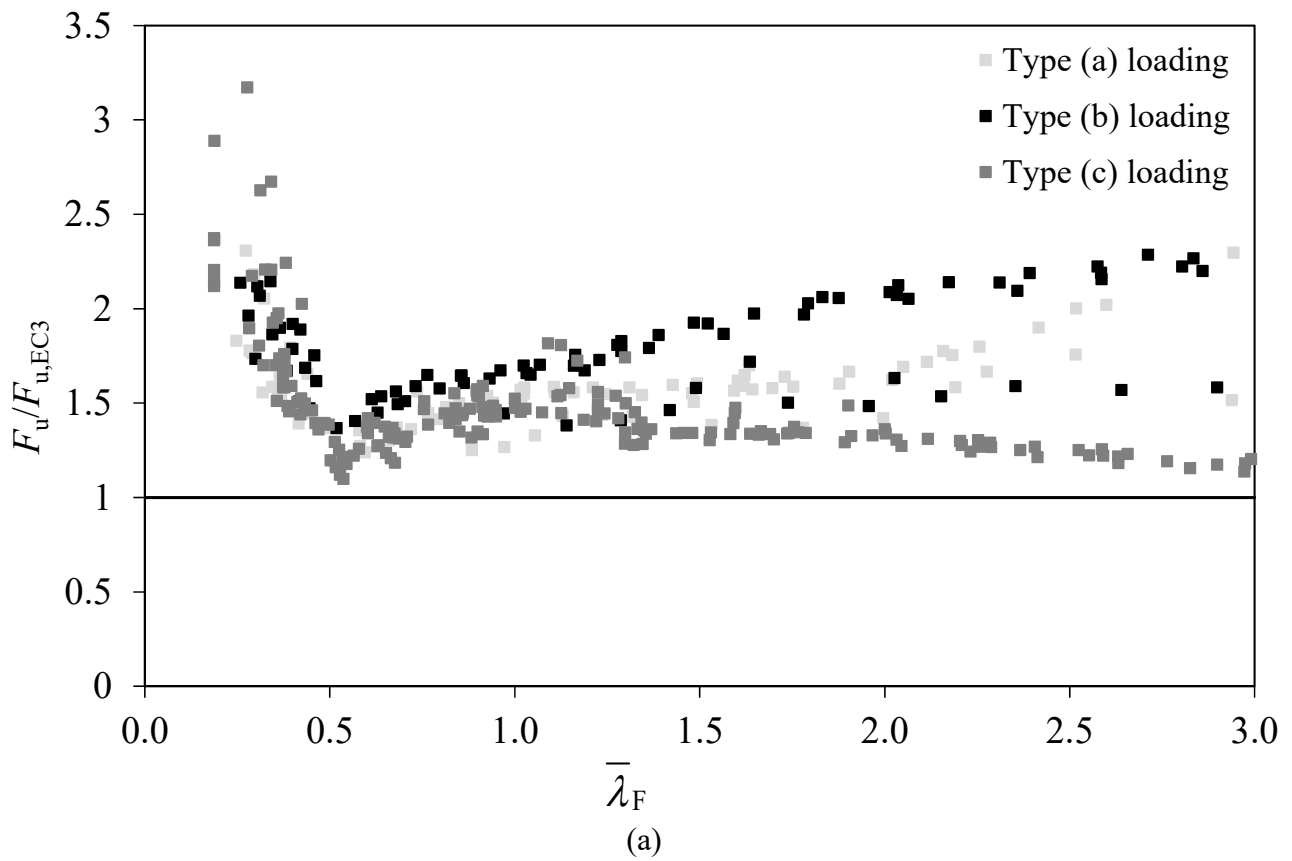


Fig. 5. Ratio of ultimate test or numerical resistance to EN 1993-1-4 predicted resistance versus slenderness (a) grouped by stainless steel type and (b) grouped by loading type.

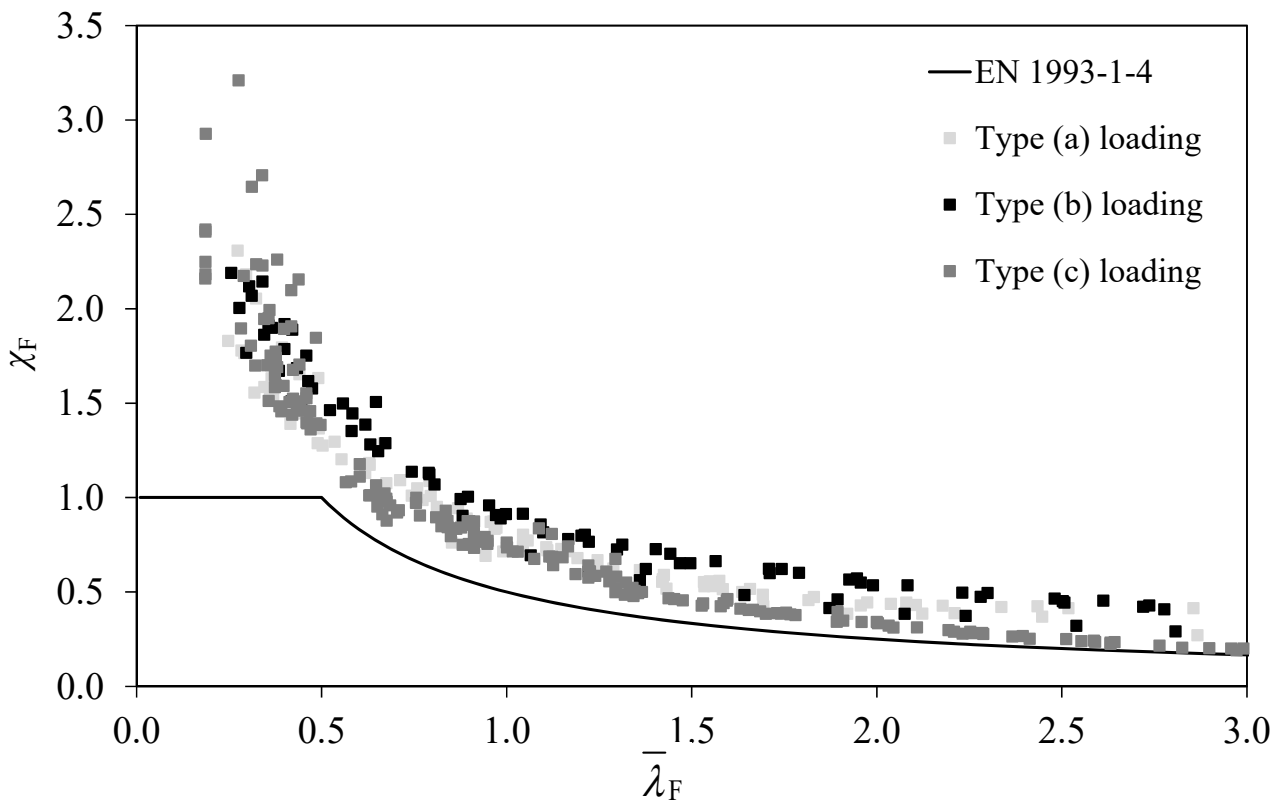


Fig. 6. Comparison of test and numerical data with EN 1993-1-4 design resistance for stainless steel members under concentrated transverse loading.

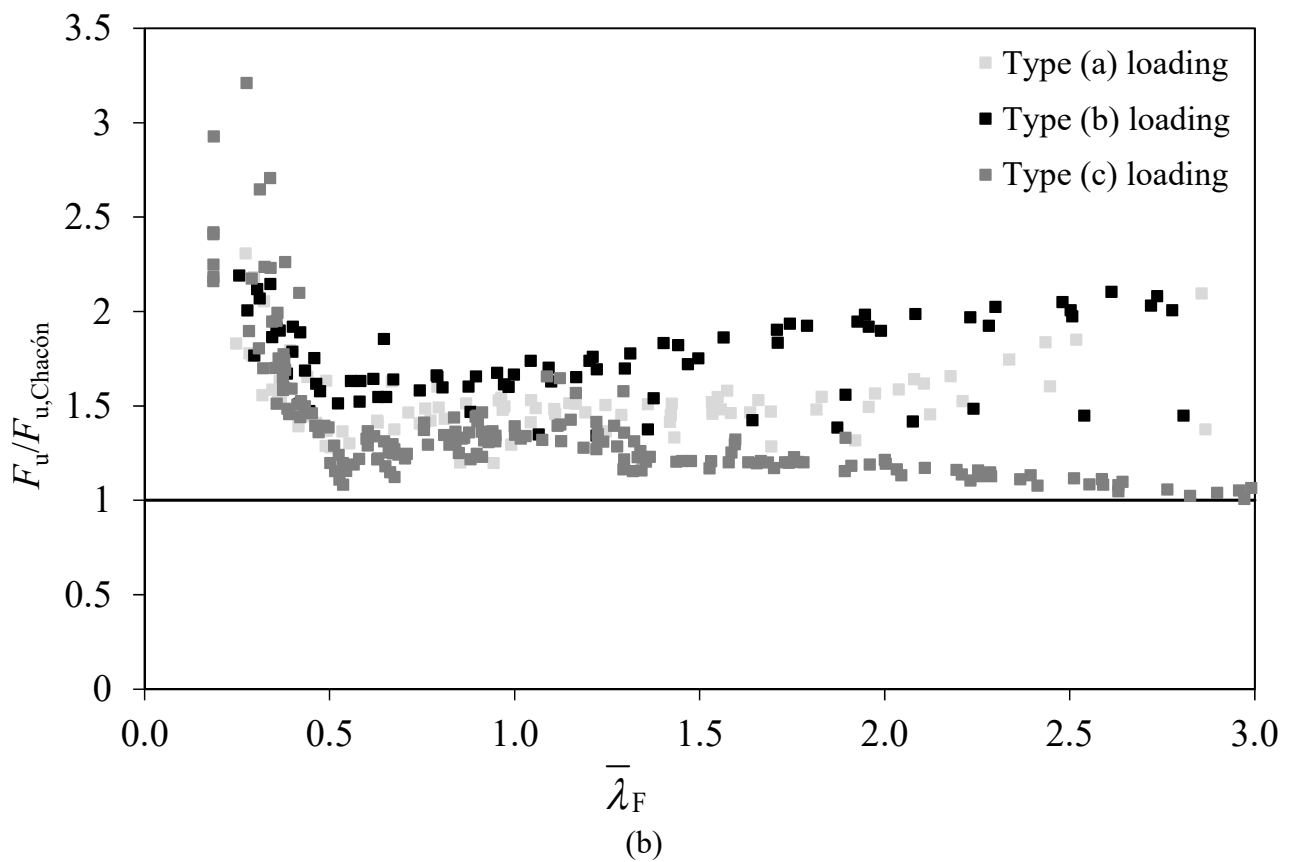
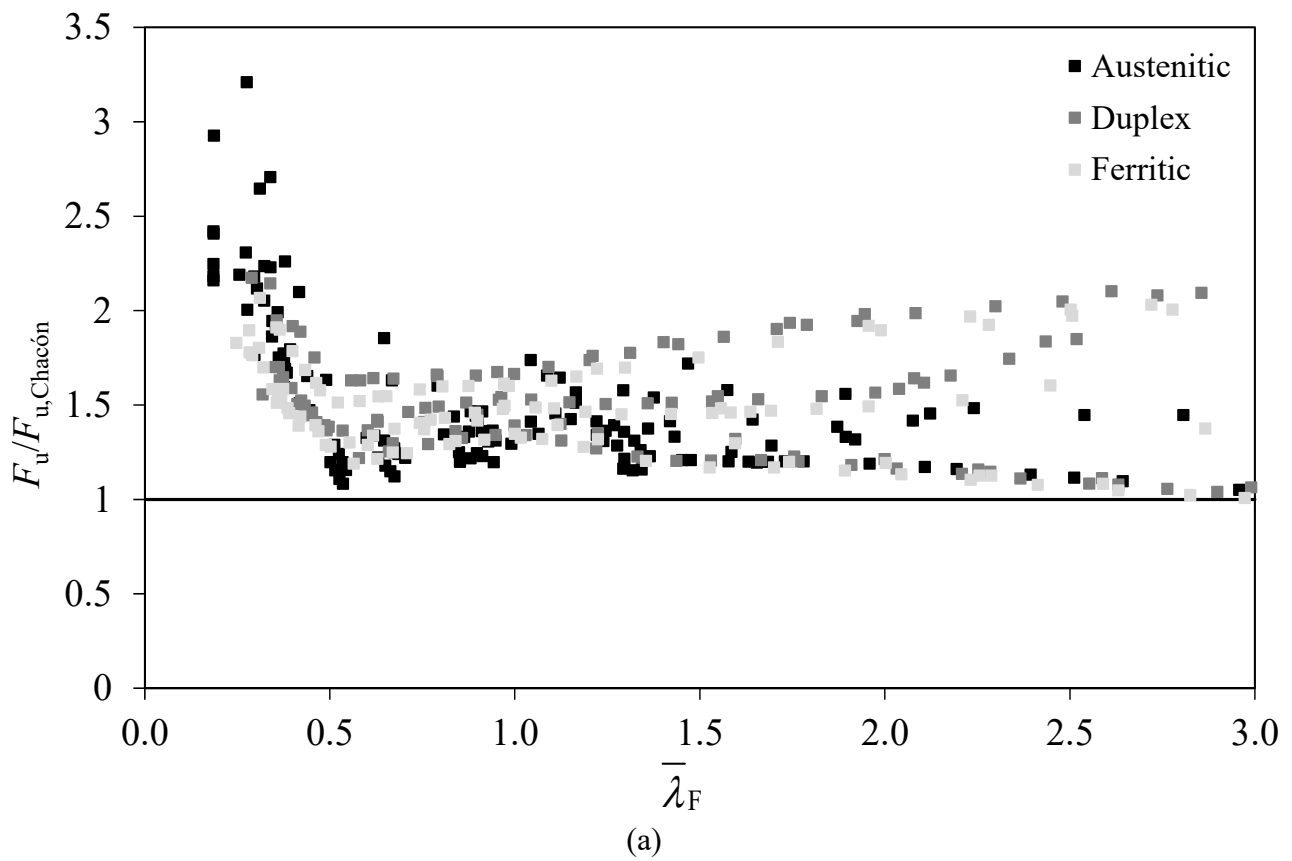


Fig. 7. Ratio of ultimate test or numerical resistance to predicted resistance from Chacón et al's proposal [4] versus slenderness (a) grouped by stainless steel type and (b) grouped by loading type.

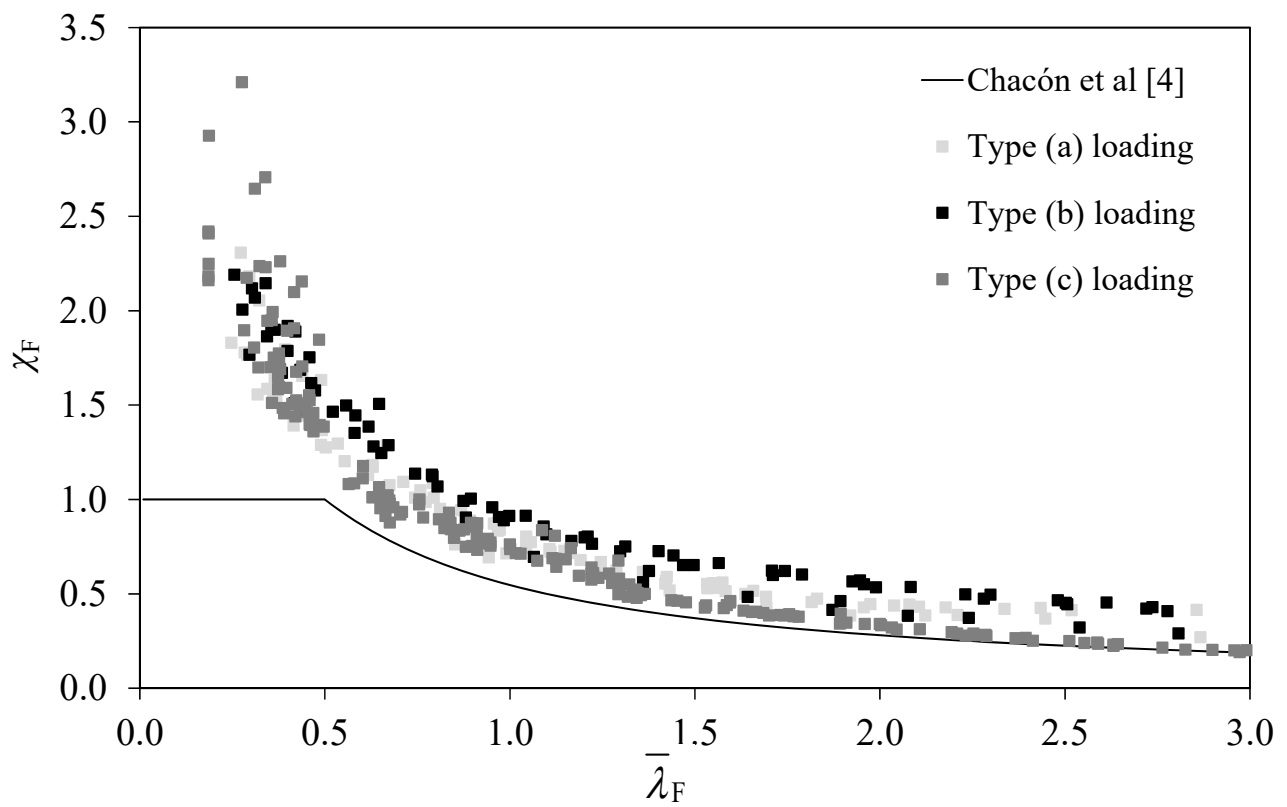


Fig. 8. Comparison of test and numerical data with Chacón et al [4] design resistance for stainless steel members under concentrated transverse loading.

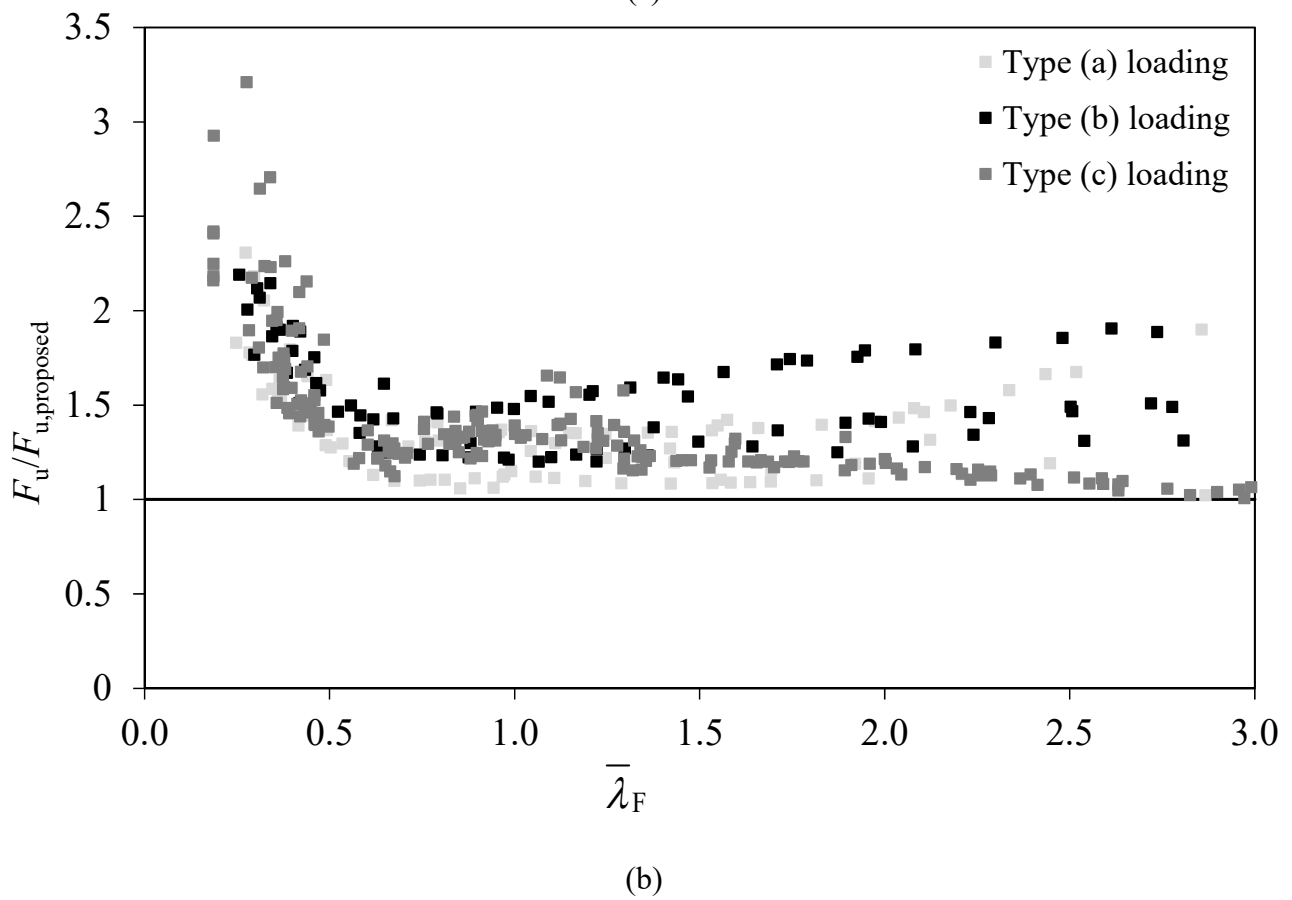
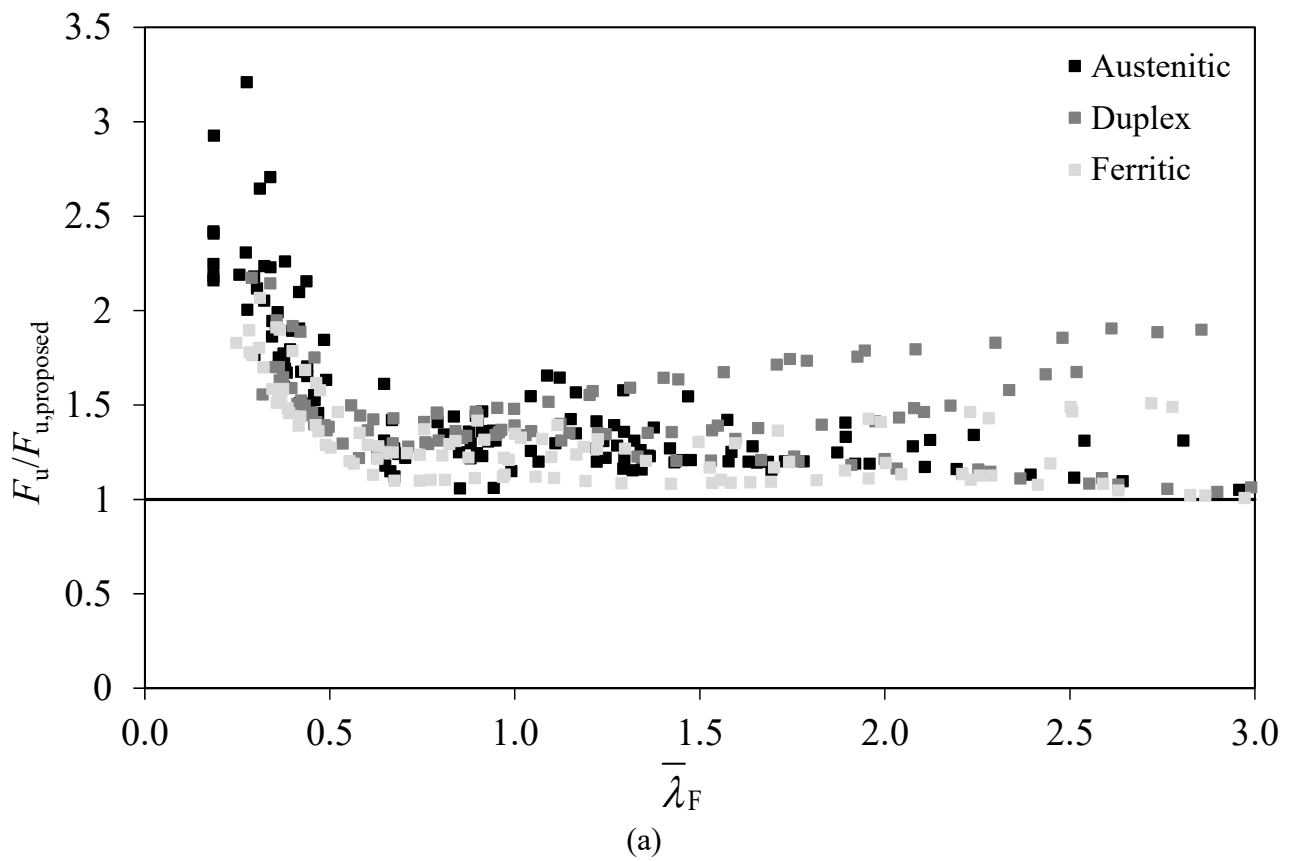


Fig. 9. Ratio of ultimate test or numerical resistance to resistance prediction from new design proposal versus slenderness (a) grouped by stainless steel type and (b) grouped by loading type.

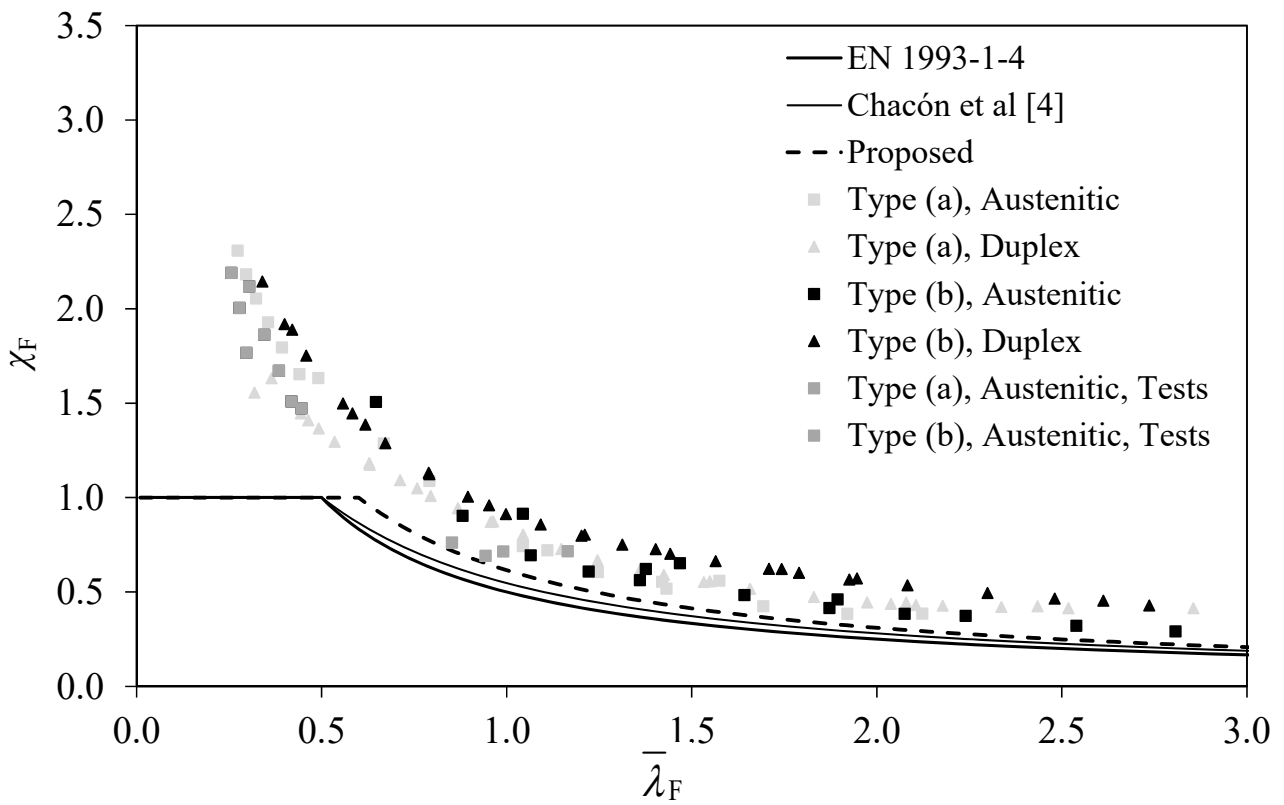


Fig. 10. Comparison of test and numerical data with proposed design resistance equations for austenitic and duplex stainless steel members under Type (a) and Type (b) concentrated loading.

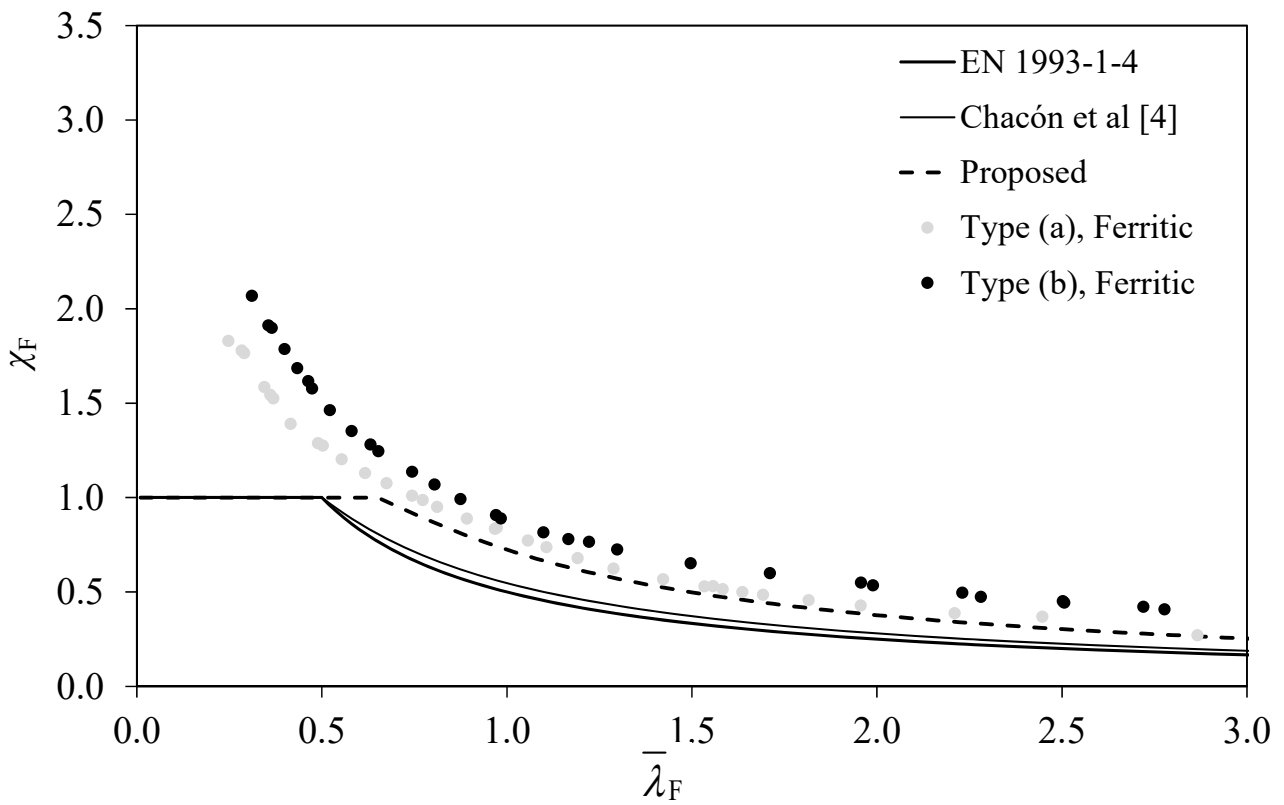


Fig. 11. Comparison of test and numerical data with proposed design resistance equations for ferritic stainless steel members under Type (a) and Type (b) concentrated loading.

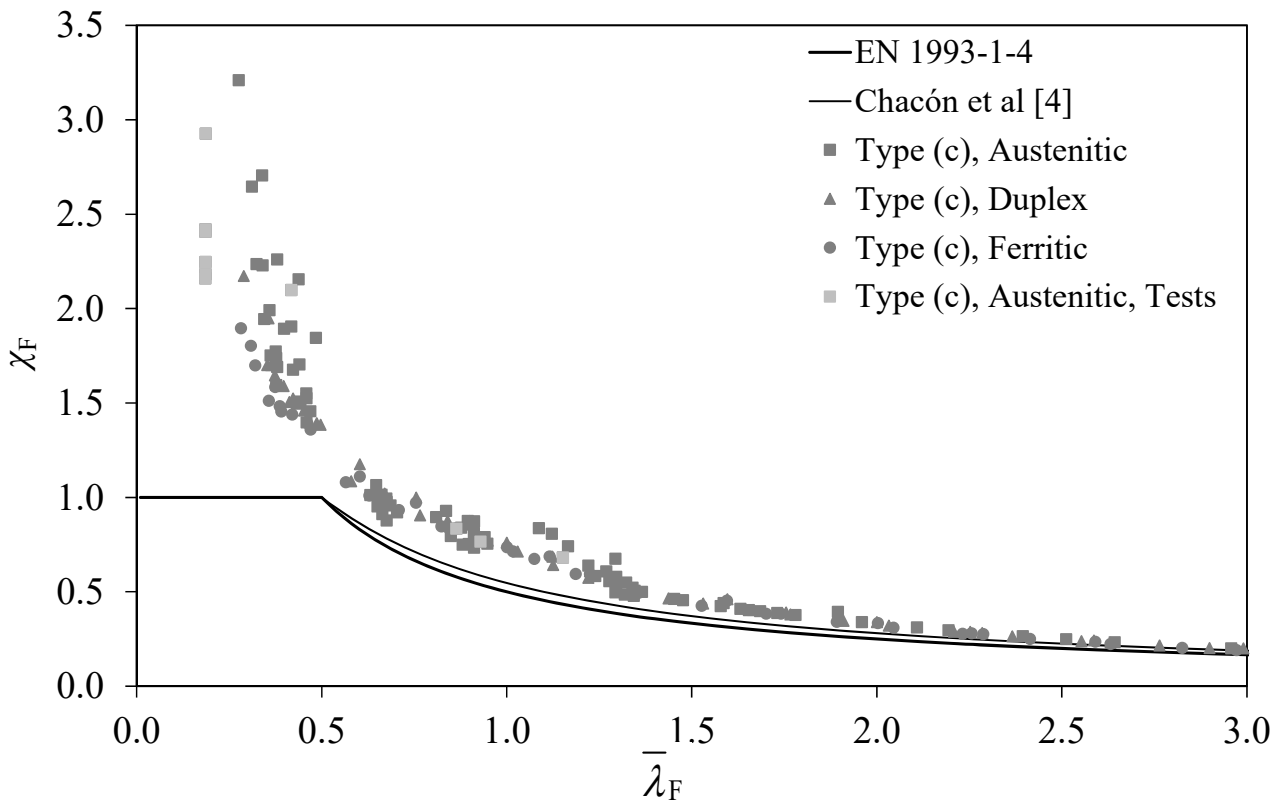


Fig. 12. Comparison of test and numerical data with proposed design resistance equations for stainless steel members under Type (c) concentrated loading.

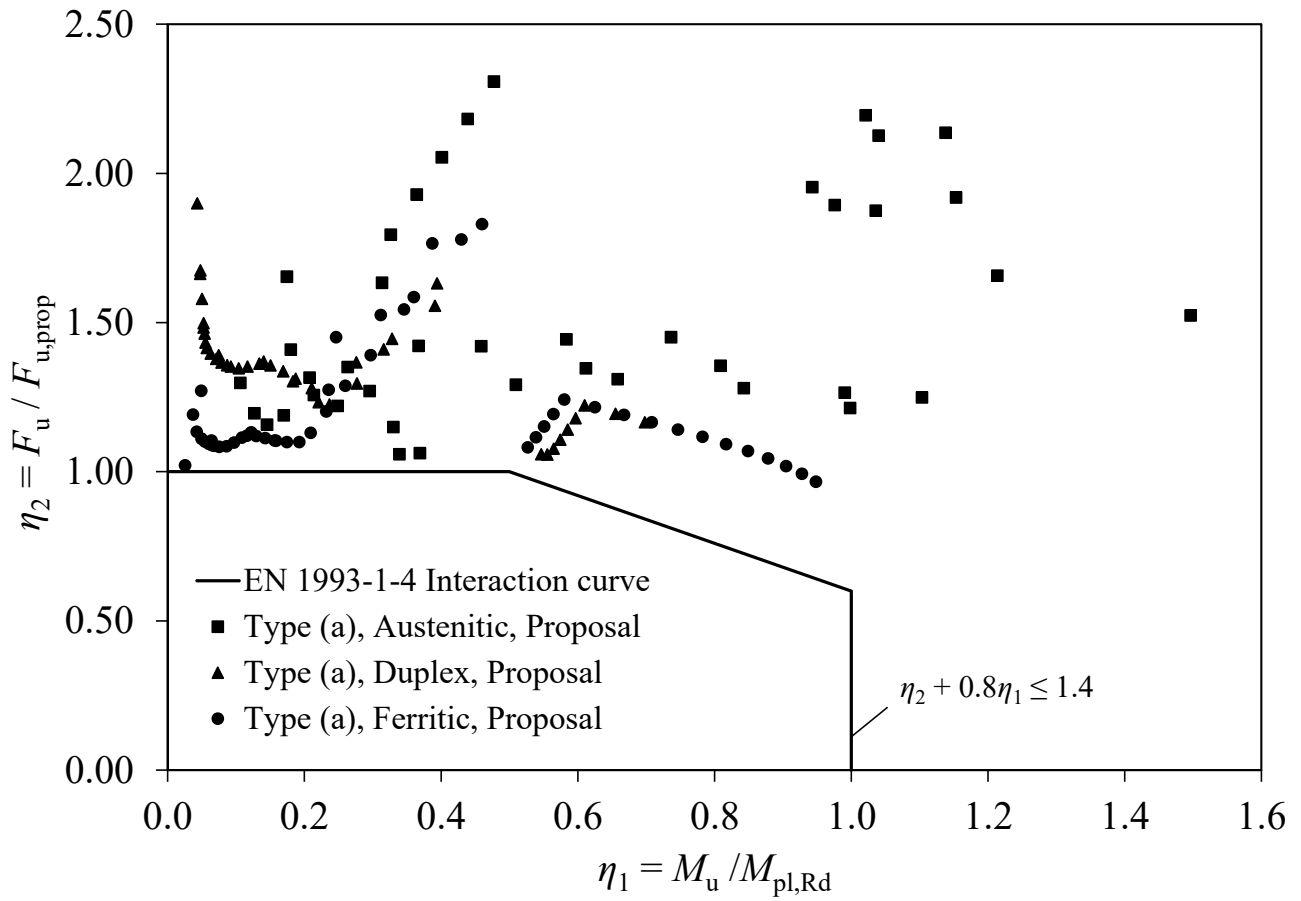


Fig. 13. Interaction curve adopted in EN 1993-1-4 for Type (a) loading together with numerical data.

**TABLES**

Table 1. Types of concentrated transverse loading investigated.

| Loading type [6] | Common description        | Diagram |
|------------------|---------------------------|---------|
| Type (a)         | Internal One-Flange (IOF) |         |
| Type (b)         | Internal Two-Flange (ITF) |         |
| Type (c)         | End One-Flange (EOF)      |         |

Table 2. Experimental database on stainless steel members subjected to concentrated transverse forces.

| Load type     | Reference                     | Label                | Grade (EN) | $f_{y,f}$            | $f_{y,w}$            | $h$   | $t_w$ | $b_f$ | $t_f$ | $s_s$ | $L$    | $a$    | $b$  | $c$ | $h_w/t_w^{(a)}$ | $F_{u,Test}$ (kN)    |
|---------------|-------------------------------|----------------------|------------|----------------------|----------------------|-------|-------|-------|-------|-------|--------|--------|------|-----|-----------------|----------------------|
|               |                               |                      |            | (N/mm <sup>2</sup> ) | (N/mm <sup>2</sup> ) | (mm)  | (mm)  | (mm)  | (mm)  | (mm)  | (mm)   | (mm)   | (mm) |     |                 |                      |
| Type (a), IOF | Sélen [10], Unosson [11]      | Pli 4301:1           | 1.4301     | 285                  | 297                  | 261.8 | 4.10  | 118.5 | 11.75 | 40.0  | 888.0  | 998.0  | –    | –   | 58.1            | 176.0                |
|               |                               | Pli 4301:2           | 1.4301     | 285                  | 297                  | 262.1 | 4.10  | 120.0 | 11.90 | 80.0  | 886.0  | 996.0  | –    | –   | 58.1            | 196.0                |
|               |                               | Pli 4301:3           | 1.4301     | 285                  | 297                  | 339.8 | 4.10  | 121.0 | 11.90 | 40.0  | 1287.0 | 1397.0 | –    | –   | 77.1            | 168.0                |
|               |                               | Pli 4301:4           | 1.4301     | 285                  | 297                  | 462.3 | 4.10  | 121.3 | 11.95 | 40.0  | 1513.0 | 1623.0 | –    | –   | 106.9           | 169.0                |
|               |                               | Pli 4301:5           | 1.4301     | 285                  | 297                  | 424.9 | 8.80  | 120.5 | 12.00 | 40.0  | 1572.0 | 1682.0 | –    | –   | 45.6            | 478.0                |
|               | dos Santos <i>et al.</i> [12] | IOF-H150-L150-SS60   | 1.4404     | 267                  | 274                  | 149.9 | 6.95  | 75.8  | 9.91  | 60.0  | 162.0  | 149.9  | –    | –   | 18.7            | 424.4 <sup>(*)</sup> |
|               |                               | IOF-H150-L200-SS60   | 1.4404     | 267                  | 274                  | 150.0 | 6.87  | 75.8  | 9.79  | 60.0  | 212.2  | 200.1  | –    | –   | 19.0            | 393.1                |
|               |                               | IOF-H150-L300-SS60   | 1.4404     | 267                  | 274                  | 149.9 | 6.88  | 75.8  | 9.76  | 60.0  | 313.1  | 301.0  | –    | –   | 19.0            | 368.6                |
|               |                               | IOF-H150-L400-SS60   | 1.4404     | 267                  | 274                  | 150.2 | 6.81  | 75.7  | 9.80  | 60.0  | 414.1  | 402.0  | –    | –   | 19.2            | 342.2                |
|               |                               | IOF-H150-L450-SS60   | 1.4404     | 267                  | 274                  | 150.0 | 6.87  | 75.7  | 9.79  | 60.0  | 464.1  | 452.0  | –    | –   | 19.0            | 340.0                |
|               |                               | IOF-H152-L150-SS30   | 1.4571     | 227                  | 272                  | 151.7 | 6.20  | 160.0 | 8.73  | 30.0  | 162.2  | 150.0  | –    | –   | 21.7            | 340.0 <sup>(*)</sup> |
|               |                               | IOF-H152-L300-SS30   | 1.4571     | 227                  | 272                  | 152.9 | 6.18  | 159.0 | 8.77  | 30.0  | 313.1  | 301.0  | –    | –   | 21.9            | 322.2 <sup>(*)</sup> |
|               |                               | IOF-H152-L450-SS30   | 1.4571     | 227                  | 272                  | 152.0 | 6.22  | 159.6 | 8.73  | 30.0  | 463.1  | 451.0  | –    | –   | 21.6            | 301.1                |
|               |                               | IOF-H152-L600-SS30   | 1.4571     | 227                  | 272                  | 152.3 | 6.18  | 159.6 | 8.88  | 30.0  | 610.1  | 598.0  | –    | –   | 21.8            | 296.7                |
|               |                               | IOF-H152-L750-SS30   | 1.4571     | 227                  | 272                  | 151.8 | 6.13  | 159.8 | 8.68  | 30.0  | 762.6  | 750.5  | –    | –   | 21.9            | 275.0                |
|               |                               | IOF-H102-L300-SS5    | 1.4571     | 222                  | 222                  | 101.4 | 4.89  | 67.9  | 5.10  | 5.0   | 311.1  | 299.0  | –    | –   | 18.6            | 126.7                |
|               |                               | IOF-H102-L300-SS7.5  | 1.4571     | 222                  | 222                  | 101.9 | 4.98  | 67.9  | 5.20  | 7.5   | 311.1  | 299.0  | –    | –   | 18.4            | 132.3                |
|               |                               | IOF-H102-L300-SS10   | 1.4571     | 222                  | 222                  | 100.8 | 4.92  | 67.8  | 5.19  | 10.0  | 311.1  | 299.0  | –    | –   | 18.4            | 121.8                |
|               |                               | IOF-H102-L300-SS12.5 | 1.4571     | 222                  | 222                  | 101.3 | 4.94  | 67.9  | 5.17  | 12.5  | 310.1  | 298.0  | –    | –   | 18.4            | 143.2                |
|               |                               | IOF-H102-L300-SS15   | 1.4571     | 222                  | 222                  | 101.9 | 4.99  | 67.8  | 5.12  | 15.0  | 310.1  | 298.0  | –    | –   | 18.4            | 130.8                |

|                       |                                      |                        |        |       |      |       |       |       |       |       |        |       |      |       |      |                    |
|-----------------------|--------------------------------------|------------------------|--------|-------|------|-------|-------|-------|-------|-------|--------|-------|------|-------|------|--------------------|
| Type<br>(b), ITF      | dos Santos<br><i>et al.</i> [12]     | IOF-H102-L300-SS20     | 1.4571 | 222   | 222  | 100.9 | 4.91  | 67.8  | 5.10  | 20.0  | 310.6  | 298.5 | –    | –     | 18.5 | 142.5              |
|                       |                                      | ITF-H102-L500-SS20     | 1.4571 | 222   | 222  | 101.3 | 4.94  | 67.8  | 4.94  | 20.0  | 524.0  | 512.0 | –    | –     | 18.5 | 154.5              |
|                       |                                      | ITF-H102-L500-SS40     | 1.4571 | 222   | 222  | 101.6 | 4.98  | 67.8  | 4.97  | 40.0  | 522.4  | 510.3 | –    | –     | 18.4 | 178.4              |
|                       |                                      | ITF-H102-L500-SS60     | 1.4571 | 222   | 222  | 101.4 | 4.94  | 67.7  | 4.92  | 60.0  | 524.4  | 512.4 | –    | –     | 18.5 | 194.8              |
|                       |                                      | ITF-H102-L500-SS80     | 1.4571 | 222   | 222  | 101.5 | 4.95  | 67.7  | 4.93  | 80.0  | 524.0  | 512.0 | –    | –     | 18.5 | 209.6              |
|                       |                                      | ITF-H102-L500-SS100    | 1.4571 | 222   | 222  | 101.6 | 5.01  | 67.8  | 4.95  | 100.0 | 524.0  | 512.0 | –    | –     | 18.3 | 239.6              |
|                       |                                      | ITF-H160-L475-SS20     | 1.4307 | 286   | 264  | 160.1 | 9.71  | 82.5  | 11.70 | 20.0  | 500.5  | 488.5 | –    | –     | 14.1 | 626.6              |
|                       |                                      | ITF-H160-L475-SS40     | 1.4307 | 286   | 264  | 160.0 | 9.72  | 82.5  | 11.75 | 40.0  | 500.1  | 488.0 | –    | –     | 14.0 | 678.8              |
|                       |                                      | ITF-H160-L475-SS60     | 1.4307 | 286   | 264  | 160.1 | 9.76  | 82.5  | 11.74 | 60.0  | 499.9  | 487.8 | –    | –     | 14.0 | 690.6              |
| Type<br>(c), EOF      | Sélen [10],<br>Unosson<br>[11]       | Ple 4301:1             | 1.4301 | 285   | 297  | 262.2 | 4.10  | 119.2 | 11.80 | 20.0  | 1000.0 | –     | 280  | 0     | 58.2 | 81.0               |
|                       |                                      | Ple 4301:2             | 1.4301 | 285   | 297  | 264.6 | 4.10  | 120.2 | 11.80 | 40.0  | 997.0  | –     | 260  | 0     | 58.8 | 102.0              |
|                       |                                      | Ple 4301:3             | 1.4301 | 285   | 297  | 340.7 | 4.10  | 118.8 | 11.75 | 60.0  | 1402.0 | –     | 419  | 0     | 77.4 | 111.0              |
|                       |                                      | Ple 4301:4             | 1.4301 | 285   | 245  | 423.6 | 8.80  | 120.6 | 11.90 | 20.0  | 1666.0 | –     | 610  | 0     | 45.4 | 258.0              |
|                       | dos Santos<br>and<br>Gardner<br>[13] | EOF-H140-b180-SS15-C0  | 1.4307 | 272   | 260  | 139.1 | 9.62  | 140.5 | 11.81 | 15.0  | 601.2  | –     | 194  | 0     | 12.0 | 367.9              |
|                       |                                      | EOF-H140-b180-SS15-C10 | 1.4307 | 272   | 260  | 139.2 | 9.61  | 140.3 | 11.78 | 15.0  | 600.7  | –     | 204  | 10    | 12.0 | 415 <sup>(x)</sup> |
|                       |                                      | EOF-H140-b180-SS15-C20 | 1.4307 | 272   | 260  | 139.1 | 9.60  | 140.3 | 11.77 | 15.0  | 601.5  | –     | 214  | 20    | 12.0 | 419 <sup>(x)</sup> |
|                       |                                      | EOF-H140-b180-SS30-C0  | 1.4307 | 272   | 260  | 139.2 | 9.62  | 140.3 | 11.78 | 30.0  | 601.0  | –     | 210  | 0     | 12.0 | 374 <sup>(x)</sup> |
|                       |                                      | EOF-H140-b180-SS30-C10 | 1.4307 | 272   | 260  | 139.3 | 9.65  | 140.3 | 11.82 | 30.0  | 600.7  | –     | 217  | 10    | 12.0 | 490 <sup>(x)</sup> |
|                       |                                      | EOF-H160-b170-SS15-C0  | 1.4307 | 286   | 264  | 160.0 | 9.77  | 82.7  | 11.74 | 15.0  | 501.0  | –     | 184  | 0     | 14.0 | 271.0              |
|                       |                                      | EOF-H160-b180-SS15-C0  | 1.4307 | 286   | 264  | 160.1 | 9.78  | 82.8  | 11.74 | 15.0  | 501.5  | –     | 192  | 0     | 14.0 | 242.3              |
|                       |                                      | EOF-H160-b190-SS15-C0  | 1.4307 | 286   | 264  | 159.9 | 9.76  | 82.6  | 11.71 | 15.0  | 501.3  | –     | 206  | 0     | 14.0 | 243.9              |
|                       |                                      | EOF-H160-b200-SS15-C0  | 1.4307 | 286   | 264  | 160.1 | 9.76  | 82.7  | 11.75 | 15.0  | 500.7  | –     | 211  | 0     | 14.0 | 269.6              |
| EOF-H160-b210-SS15-C0 | 1.4307                               | 286                    | 264    | 160.0 | 9.76 | 82.8  | 11.74 | 15.0  | 500.8 | –     | 221    | 0     | 14.0 | 251.7 |      |                    |

– Not applicable.

<sup>(i)</sup>  $h_w = h - 2 \times t_f$

<sup>(x)</sup> Critical design check was combined bending and shear force. This result was not considered in the assessment and proposal of design curves for concentrated loading.

<sup>(\*)</sup> Critical design check was shear force. This result was not considered in the assessment and proposal of design curves for concentrated loading.

Table 3. Material properties adopted for numerical studies.

| Material grade                           | $E$                  | $f_y$                | $f_u$                | $\epsilon_u$ | Ramberg-Osgood parameters |      |
|--|----------------------|----------------------|----------------------|--------------|---------------------------|------|
|  | (N/mm <sup>2</sup> ) | (N/mm <sup>2</sup> ) | (N/mm <sup>2</sup> ) | (%)          | $n$                       | $m$  |
| Austenitic<br>(see I 102×68×5×5 in [13]) | 186800               | 222                  | 580                  | 50           | 3.1*                      | 3.9* |
| Duplex<br>(see ref. [26])                | 200000               | 530                  | 770                  | 30           | 9.3                       | 3.6  |
| Ferritic<br>(see ref. [26])              | 200000               | 320                  | 480                  | 16           | 17.2                      | 2.8  |

\* Average of measured material properties from tensile coupon tests adopted in validation and parametric studies.

Table 4. Boundary conditions adopted in finite element models.

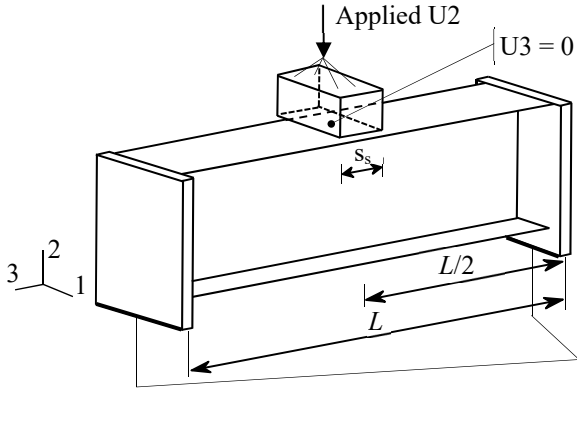
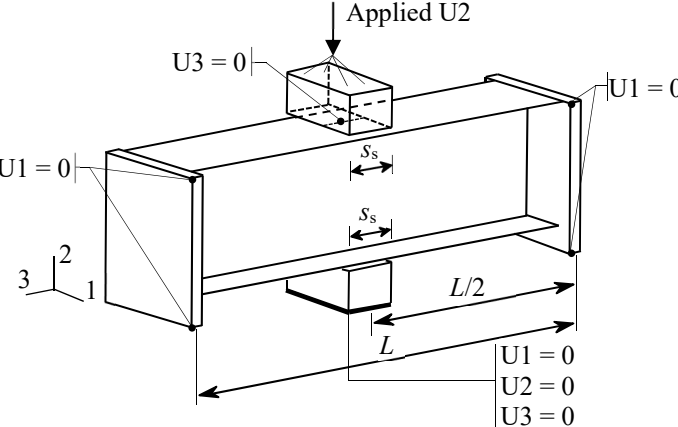
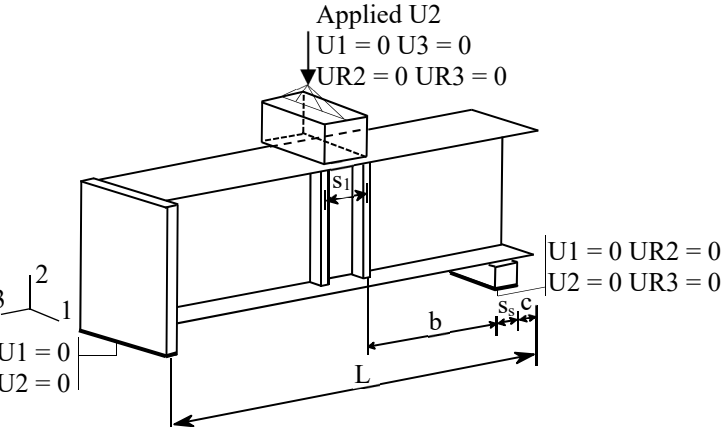
| Loading type | Boundary conditions   |
|--------------|---|
| Type (a)     |  <p>Applied <math>U_2</math></p> <p><math>U_3 = 0</math></p> <p><math>s_s</math></p> <p><math>L/2</math></p> <p><math>L</math></p> <p><math>U_1 = 0</math><br/> <math>U_2 = 0</math><br/> <math>UR_2 = 0</math><br/> <math>UR_3 = 0</math></p>  |
| Type (b)     |  <p>Applied <math>U_2</math></p> <p><math>U_3 = 0</math></p> <p><math>U_1 = 0</math></p> <p><math>s_s</math></p> <p><math>s_s</math></p> <p><math>L/2</math></p> <p><math>L</math></p> <p><math>U_1 = 0</math><br/> <math>U_2 = 0</math><br/> <math>U_3 = 0</math></p>   |
| Type (c)     |  <p>Applied <math>U_2</math></p> <p><math>U_1 = 0</math> <math>U_3 = 0</math><br/> <math>UR_2 = 0</math> <math>UR_3 = 0</math></p> <p><math>s_1</math></p> <p><math>b</math></p> <p><math>s_s</math> <math>c</math></p> <p><math>L</math></p> <p><math>U_1 = 0</math> <math>UR_2 = 0</math><br/> <math>U_2 = 0</math> <math>UR_3 = 0</math></p> |

Table 5. Summary of comparisons between test and FE results for imperfection amplitude of  $t_w/500$  [12, 13].

| Loading type        | No. of tests | $F_{u,FE}/F_{u,test}$ for $\omega = t_w/500$ |      |
|---------------------|--------------|--|------|
|                     |              | Mean   | COV  |
| Type (a), ref. [12] | 16           | 1.01   | 0.04 |
| Type (b), ref. [12] | 8            | 0.96   | 0.04 |
| Type (c), ref. [13] | 10           | 1.01   | 0.13 |

Table 6. Summary of evaluation of current design procedure in EN 1993-1-4 [14] for stainless steel members under concentrated transverse loading.

| Loading type | $F_u/F_{u,EC3}$ |      |      |   |      |      |  |      |      |
|--------------|-----------------|------|------|---|------|------|--|------|------|
|              | All cases       |      |      | $\bar{\lambda}_F \leq \bar{\lambda}_{F0}$ |      |      | $\bar{\lambda}_F > \bar{\lambda}_{F0}$ |      |      |
|              | n               | Mean | COV  | n   | Mean | COV  | n                                      | Mean | COV  |
| Type (a)     | 140             | 1.50 | 0.11 | 72  | 1.45 | 0.10 | 68                                     | 1.56 | 0.12 |
| Type (b)     | 83              | 1.79 | 0.13 | 23  | 1.76 | 0.13 | 60                                     | 1.81 | 0.11 |
| Type (c)     | 182             | 1.48 | 0.19 | 53  | 1.74 | 0.17 | 129                                    | 1.37 | 0.09 |

Table 7. Summary of evaluation of Chacón et al. [4] design procedure applied to stainless steel members under concentrated transverse loading.

| Loading type | $F_u/F_{u,Chacón}$ |      |      |   |      |      |  |      |      |
|--------------|--------------------|------|------|---|------|------|--|------|------|
|              | All cases          |      |      | $\bar{\lambda}_F \leq \bar{\lambda}_{F0}$ |      |      | $\bar{\lambda}_F > \bar{\lambda}_{F0}$ |      |      |
|              | n                  | Mean | COV  | n   | Mean | COV  | n                                      | Mean | COV  |
| Type (a)     | 140                | 1.45 | 0.12 | 72  | 1.41 | 0.13 | 68                                     | 1.49 | 0.07 |
| Type (b)     | 83                 | 1.74 | 0.11 | 23  | 1.79 | 0.12 | 60                                     | 1.73 | 0.09 |
| Type (c)     | 182                | 1.40 | 0.23 | 53  | 1.75 | 0.24 | 129                                    | 1.25 | 0.10 |

Table 8. Values of  $\alpha_{F0}$  and  $\bar{\lambda}_{F0}$  for  $\gamma_{M1} = 1.10$  (proposed design approach).

| Loading type | Austenitic and Duplex |                      | Ferritic      |                      |
|--------------|-----------------------|----------------------|---------------|----------------------|
|              | $\alpha_{F0}$         | $\bar{\lambda}_{F0}$ | $\alpha_{F0}$ | $\bar{\lambda}_{F0}$ |
| Type (a)     | 0.60                  | 0.60                 | 0.30          | 0.65                 |
| Type (b)     |                       |                      |               |                      |
| Type (c)     | 0.75                  | 0.50                 | 0.75          | 0.50                 |

Table 9. Summary of evaluation of proposed design method for stainless steel members under concentrated transverse loading.

| Loading type | $F_u/F_{u,prop}$ |      |      |   |      |      |  |      |      |
|--------------|------------------|------|------|---|------|------|--|------|------|
|              | All cases        |      |      | $\bar{\lambda}_F \leq \bar{\lambda}_{F0}$ |      |      | $\bar{\lambda}_F > \bar{\lambda}_{F0}$ |      |      |
|              | n                | Mean | COV  | n   | Mean | COV  | n                                      | Mean | COV  |
| Type (a)     | 140              | 1.37 | 0.14 | 72  | 1.47 | 0.10 | 68                                     | 1.26 | 0.07 |
| Type (b)     | 83               | 1.54 | 0.15 | 23  | 1.77 | 0.14 | 60                                     | 1.46 | 0.09 |
| Type (c)     | 182              | 1.43 | 0.23 | 53  | 1.85 | 0.18 | 129                                    | 1.25 | 0.10 |

Table 10. Summary of reliability analysis results for design expressions for stainless steel members under concentrated transverse loading.

| Load type                      | Material   | $\alpha_{F0}$ | $\bar{\lambda}_{F0}$ | $n$ | $b$   | $f_{y,mean}/f_{y,nom}$ | $V_{\delta}$ | $V_{fyw}$ | $V_{tw}$ | $V_{rt}$ | $V_{FEM}$ | $k_{d,n}$ | $\gamma_{M1}$ |
|--------------------------------|------------|---------------|----------------------|-----|-------|------------------------|--------------|-----------|----------|----------|-----------|-----------|---------------|
| Type (a), $M_u < 0.5M_{pl}$    | Austenitic | 0.60          | 0.60                 | 15  | 1.252 | 1.30                   | 0.095        | 0.060     | 0.050    | 0.089    | 0.040     | 3.44      | 1.08          |
|                                | Duplex     | 0.60          | 0.60                 | 26  | 1.416 | 1.10                   | 0.105        | 0.030     | 0.050    | 0.082    | 0.040     | 3.44      | 1.05          |
|                                | Ferritic   | 0.30          | 0.65                 | 23  | 1.106 | 1.20                   | 0.027        | 0.045     | 0.050    | 0.077    | 0.040     | 3.44      | 1.05          |
| Type (a), $M_u \geq 0.5M_{pl}$ | Austenitic | 0.60          | 0.60                 | 19  | 1.697 | 1.30                   | 0.191        | 0.060     | 0.050    | 0.062    | 0.040     | 3.44      | 0.96          |
|                                | Duplex     | 0.60          | 0.60                 | 18  | 1.192 | 1.10                   | 0.052        | 0.030     | 0.050    | 0.037    | 0.040     | 3.44      | 0.94          |
|                                | Ferritic   | 0.30          | 0.65                 | 16  | 1.214 | 1.20                   | 0.043        | 0.045     | 0.050    | 0.045    | 0.040     | 3.44      | 0.85          |
| Type (b)                       | Austenitic | 0.60          | 0.60                 | 15  | 1.347 | 1.30                   | 0.096        | 0.060     | 0.050    | 0.099    | 0.040     | 3.44      | 1.00          |
|                                | Duplex     | 0.60          | 0.60                 | 24  | 1.642 | 1.10                   | 0.096        | 0.030     | 0.050    | 0.091    | 0.040     | 3.44      | 0.88          |
|                                | Ferritic   | 0.30          | 0.65                 | 21  | 1.334 | 1.20                   | 0.082        | 0.045     | 0.050    | 0.087    | 0.040     | 3.44      | 0.98          |
| Type (c)                       | Austenitic | 0.75          | 0.50                 | 61  | 1.281 | 1.30                   | 0.100        | 0.060     | 0.050    | 0.099    | 0.130     | 3.44      | 0.97          |
|                                | Duplex     | 0.75          | 0.50                 | 36  | 1.237 | 1.10                   | 0.091        | 0.030     | 0.050    | 0.093    | 0.130     | 3.44      | 1.04          |
|                                | Ferritic   | 0.75          | 0.50                 | 32  | 1.219 | 1.20                   | 0.091        | 0.045     | 0.050    | 0.094    | 0.130     | 3.44      | 1.01          |